Research Square

Preprints are preliminary reports that have not undergone peer review.
They should not be considered conclusive, used to inform clinical practice,
or referenced by the media as validated information.

Multi-Scale Modeling of the Effects of Optimizing Speed Bumps and Speed Humps on Patients, Occupants, and Drivers: A Convolutional Neural Network and Biomechanical Modeling Approach

Sayyedmehdi Hosseinikhah

sayyedmehdihosseinikhah@gmail.com

Ki.C, Islamic Azad University

Hamid Mirzahossein

Imam Khomeini International University (IKIU)

Mohammad Ali Asadi

S.C, Islamic Azad University

Ali Naderan

SR.C, Islamic Azad University

Article

Keywords: Speed bump, Speed hump, Patients, Occupants, Drivers, Convolutional Neural Network

Posted Date: November 13th, 2026

DOI: https://doi.org/10.21203/rs.3.rs-11440279/v1

License: This work is licensed under a Creative Commons Attribution 4.0 International License.
Read Full License

Additional Declarations: No competing interests reported.

Multi-Scale Modeling of the Effects of Optimizing Speed Bumps and Speed Humps on Patients, Occupants, and Drivers: A Convolutional Neural Network and Biomechanical Modeling Approach

Sayyedmehdi Hosseinikhah[a]*, Hamid Mirzahossein[b], Mohammad Ali Asadi[c], Ali Naderan[d]

[a]Department of Civil Engineering, Ki.C.,Islamic Azad University, Kish, Iran

Civil Engineering Expert, Shiraz Central Municipality, Shiraz, Iran

sayyedmehdihosseinikhah@gmail.com

[b]Department of Civil - Transportation Planning, Imam Khomeini International University (IKIU). Qazvin, Iran

Mirzahossein@eng.ikiu.ac.ir

[c]Department of Computer Engineering, S.C., Islamic Azad University, Shiraz, Iran

Ma.asadi@iau.ac.ir

[d]Department of Civil Engineering, SR.C., Islamic Azad University, Tehran, Iran

Naderan@iau.ac.ir

Abstract

Traffic calming is recognized as a set of physical interventions aimed at reducing vehicle speeds and enhancing the safety of vulnerable road users. However, speed bumps and speed humps can exert considerable adverse effects on patients, occupants, and drivers. This study aimed to conduct multi-scale modeling of the effects of optimizing the number and location of speed bumps and speed humps on these three groups. To this end, a convolutional neural network was employed to determine the optimal number of obstacles across 48 urban roadways. Subsequently, the effects of reducing obstacles on eight patient groups (cardiovascular, spinal, intubated, CPR, post-surgical, pregnant women, osteoporosis, and stroke) and on occupant and driver groups were quantified using biomechanical and clinical models. The results indicated that scenario S5, with 39 speed bumps and 45 speed humps, exhibits the best performance, achieving a 51.3% reduction in the number of speed bumps and a 55.9% reduction in the number of speed humps compared with the existing condition. This reduction led to a 51.7% decrease in the cumulative driver anger index, a 51.3% reduction in zero occupant comfort, a 42.6% reduction in cardiovascular risk, a 66.7% reduction in endotracheal tube displacement, and a 45.5% improvement in CPR quality. Dynamic analysis using the reference vehicle demonstrated that although the road acceleration at speed bumps is 16.8 times that at speed humps, due to suspension damping, the actual acceleration on the vehicle seat is only 22.8 times greater, and the actual VDV is approximately 3.3 times greater. The findings indicate that reducing the number of speed bumps takes higher priority than reducing speed humps.

Keywords: Speed bump, Speed hump, Patients, Occupants, Drivers, Convolutional Neural Network

*Corresponding Author

1. Introduction

Traffic calming, as one of the principal strategies in traffic engineering and urban roadway design, is recognized for its objectives of moderating vehicle speeds, reducing crash severity, and restoring safety for vulnerable road users such as pedestrians [1,2]. Within the classification of physical calming devices, vertical deflection measures particularly speed bumps and speed humps account for the largest share of traffic management in residential areas and around educational centers, owing to their rapid implementation and immediate deterrent effect on driver speeds [3, 4, 5]. Nevertheless, the geometric distinction between these two devices produces markedly different dynamic effects; speed bumps, with their short width (typically less than one meter) and steep slopes, generate severe impacts, whereas speed humps, with their greater length (more than 3.5 meters), enable safer passage at controlled speeds [6, 7].

The dense installation and improper siting of these obstacles in recent decades have given rise to the phenomenon of speed bump saturation in urban networks. This phenomenon has not only led to increased braking and repeated acceleration, fuel wastage, and greenhouse gas emissions [8, 9], but has also created cascading disruptions in free-flowing traffic. A more critical and overlooked challenge concerns the adverse consequences of these obstacles for the emergency medical services (EMS) fleet and the health of patients being transported [10, 11]. Field studies have demonstrated that traversing each vertical obstacle imposes an average direct delay of 3 to 10 seconds on emergency vehicle movement, and in the event of traffic queue formation behind the obstacles, this time loss can reach tens of seconds [12]. In medical emergencies such as cardiac arrest, stroke, and major trauma where the critical concept of the Golden Hour determines patient survival every one-minute delay in emergency response increases the risk of mortality by between 8 and 17 percent [13, 14, 15].

From a biomechanical perspective and in accordance with whole-body vibration standards [16], accelerated traversal of speed bumps imposes destructive dynamic stresses on occupants [17, 18, 19]. The instantaneous vertical acceleration and the rate of sudden change in acceleration, or jerk, exert an increasing axial compressive load on the spine and, in patients with disc herniation, orthopedic fractures, or vertebral instability, can lead to irreversible spinal injuries [20]. Furthermore, during patient transport by ambulance, severe vibrations and vertical impulses caused by speed bumps severely degrade the quality of cardiopulmonary resuscitation (CPR), disrupting the standard depth and rhythm of chest compressions by medical personnel [21, 22, 23]. These forces can also, through kinetic stimulation, cause dislodgement of angiocatheters and endotracheal tubes, elevate intracranial pressure (ICP) in brain trauma, and exacerbate renal pain.

In parallel with the complexity of the roadway network, traditional decision-making approaches based on local site visits or qualitative judgments by traffic engineers have revealed their inefficacy in resolving this conflict of interests. In recent years, the application of artificial intelligence (AI), computational modeling, and machine learning (ML) algorithms has brought about a remarkable transformation in the analysis of calming-related impacts. One branch of this research has employed convolutional neural networks (CNNs) and computer vision to detect and extract the spatial locations of speed bumps and monitor their geometric characteristics via smartphone sensors or vehicle-mounted imagery [24, 25, 26]. In the field of traffic engineering, multilayer perceptrons (MLPs) and ensemble deep learning algorithms have been employed

to predict 85th-percentile speeds, model the nonlinear response of suspension systems, and optimize the geometric profiles of obstacles [27,28,29]. These learning-based models are capable of identifying undesirable obstacle placement patterns and extracting optimal network configurations by analyzing complex, multidimensional relationships among traffic volume, roadway functional classification, access to medical centers, and crash risk.

Despite the extensive development of AI-based models, the existing literature faces a fundamental research gap: most previous AI studies have been confined either to the problem of computer vision (obstacle detection) or to single-objective optimization of vehicle speeds, and none of the deep learning models have addressed the optimal placement of speed bumps/humps, nor have they considered secondary human consequences including occupant vibration dose, patient biomechanical shock, and ambulance golden-hour time loss as evaluation criteria.

The main innovations of this research are as follows:

Deployment and comparison of four distinct neural network architectures with the existing roadway condition and expert opinions for redesigning and optimizing the layout of speed bumps and humps across a real network comprising 48 urban roadways.

Development of a multi-criteria analytical framework that requires no invasive clinical data, for transforming optimization outputs into standard biomechanical indicators (in accordance with ISO 2631-1), skeletal compressive force, patient shock index, and rescue survival probability.

Quantitative model-based demonstration of the superior performance of the neural network approach in simultaneously reducing redundant speed control measures, shortening emergency fleet arrival times, and decreasing the biomechanical burden imposed on patients, compared with both the existing condition and human expert judgment.

Following the introduction, Section 2 of this paper is dedicated to the methodology, encompassing data collection, neural network optimization, and biomechanical modeling. Section 3 presents the computational results for eight patient groups and two occupant and driver groups. Subsequently, the discussion section interprets the findings and compares them with the existing literature, and finally, the conclusion provides a final synthesis.

2. Methodology

This section describes the methodological framework of the research in four consecutive steps. The first step is dedicated to the collection of traffic and urban data. The second step addresses the evaluation and weighting of criteria. The third step explains the architecture and implementation of the deep neural network model, and the fourth step deals with modeling the effects on patients, occupants, and drivers. These four steps are designed in a sequential chain to progress from raw primary data to the final optimized model.

Step One: Collection of Traffic and Urban Data

Data collection in this study involved identifying data sources from road facilities and the municipality, specifying information recording instruments, and monitoring data through normalization, noise removal, and conversion of qualitative data into quantitative form. Raw data were gathered from various sources over a six-month period. These sources included: municipalities and the transportation organization, which provided data on traffic volume, speed, number of lanes, street width, gradient, and speed bump locations; the traffic control center, which supplied instantaneous speed and camera data; the traffic police, which recorded crash statistics; and the urban planning department, which provided land-use and parking information.

In addition to recorded data, field surveys were conducted to measure speed bump dimensions, equipment spacing, and manual counts for validation purposes. Spatial data were extracted from GIS layers and satellite imagery. Data preprocessing included outlier removal, normalization, noise removal, and conversion of qualitative data into quantitative form. Out of 146 roadways under study, after applying quality filters, 116 roadways with complete data were selected. For each roadway, 16 primary criteria and 35 sub-criteria were identified and quantified.

Step Two: Evaluation and Weighting of Criteria and Sub-Criteria

The input data for this step were collected through geometric surveys, recording of traffic volume and speed, crash histories, and residents' opinions. In the weighting phase, experts' opinions were first harmonized using the Delphi method, and then the final weights of the indicators were determined using the Analytic Hierarchy Process (AHP) based on pairwise comparisons. Through a review of the scientific literature and the participation of a panel of domestic experts including traffic engineers, urban planners, safety officials, and researchers via several Delphi rounds and group discussions, a hierarchical evaluation system comprising 16 primary criteria and 35 sub-criteria was developed, and quantitative scores and importance coefficients were assigned to each criterion.

The feature vector is a numerical representation of the status of each roadway segment and, based on data from 116 roadways and the evaluation criteria, is composed of three groups. The first group comprises continuous features, including 16 features that encompass the numerical scores of the 16 primary roadway evaluation criteria and are directly used as model inputs. The second group comprises categorical features, including 229 features that cover the characteristics of trip-attracting land uses along the roadway and adjacent roadways such as commercial, medical, and office land uses as well as roadway characteristics including gradient, roundabout, and service or access roads. The type of each feature and its distance from the beginning of the roadway were recorded. The third group comprises supplementary geometric and traffic features, including 12 features that encompass information on crash locations along the roadway, the posted speed limit, and the roadway length. In total, a 257-dimensional feature vector was extracted from the scoring system.

Step Three: Architecture and Implementation of the Deep Neural Network Model

This step examines various deep neural network models and analyzes the selected network architecture. The deep neural network architecture was selected for its capability to recognize complex features. Three common architectures were systematically compared. The Multilayer Perceptron (MLP) model was considered as the baseline model for learning nonlinear relationships, without capturing spatial or temporal patterns. The Long Short-Term Memory (LSTM) model was evaluated as suitable for sequential data and for capturing long-term dependencies in time series. The Convolutional Neural Network (CNN) model was examined for automatically extracting hierarchical and spatial features from input data using convolutional layers.

Performance evaluation criteria included MSE, RMSE, MAE, and R^2 (Equations 1 to 4). All models were trained under identical conditions and with identical datasets and evaluated on independent test data. The CNN model demonstrated superior performance, with the highest R^2 and the lowest squared errors. It also exhibited higher spatial accuracy, whereas the MLP and LSTM models occasionally predicted speed bumps outside the roadway boundaries. The CNN produced no such errors, and all predictions fell within the logical range of the roadway length. This advantage makes the CNN the preferred choice for real-world traffic management applications where geographic accuracy is critical.

$$MSE = \frac{1}{n} + \sum_{i=1}^{n} (Y_i - \hat{Y}_i)^2 \quad (1)$$

$$R_{MSE} = \sqrt{\frac{\sum (y_i - \hat{Y}_i)^2}{n}} \quad (2)$$

$$MAE = \frac{|Y_i - \hat{Y}_i|}{n} \quad (3)$$

$$R^2 = 1 - \frac{SSE(Sum\ of\ Squared\ Errors)}{SST(total\ sum\ of\ squares)} \quad (4)$$

With 5-fold cross-validation, the CNN demonstrated superior performance compared to MLP and LSTM and exhibited the lowest variance. In sensitivity analysis under Gaussian noise at levels of 0.05 and 0.10 and feature masking at 10% and 20%, the CNN was the most robust. For instance, under noise with a standard deviation of 0.10, the CNN was able to retain 91% of its baseline R^2, and with 20% feature masking, it maintained 89% of its initial accuracy. Meanwhile, the MLP retained only 76% and 68%, and the LSTM only 79% and 73%, of their initial accuracy.

The input data for this study comprise 257 features extracted from 116 urban roadways, which, after preprocessing and normalization, were provided to the neural network as a comprehensive feature vector. For network training (68 roadways), four independent reference groups were used. The first group was the existing condition of the roadways, including the locations of currently installed speed bumps and humps. The second group comprised the opinions of the first expert (a traffic specialist with 10 years of experience).

The third group included the opinions of the second expert (a specialist in safety and urban planning). The fourth group was the combination of the three previous groups, considered as the expert consensus and the final reference. Thus, a total of four independent training models were trained on an identical input dataset so that the performance of each model could be compared separately against different references.

After training the four models, the test data comprising 48 roadways not used in the training process were fed to all four models, and the output of each model was generated as 10 separate outputs for each roadway. These 10 outputs represent 10 proposed locations for the installation of calming devices on each roadway. Subsequently, the output of each model was compared with three independent references: the existing condition of the roadways, the opinion of the first expert, and the opinion of the second expert. Thus, a total of seven comparison groups were formed: four neural network models versus three references.

To ensure the absence of overfitting in the models, three principal strategies were employed. First, the data were randomly and without overlap divided into three sets: training (68 roadways), validation (20 roadways), and testing (48 roadways). Second, Early Stopping with a patience of 50 epochs was used, such that training is halted if the validation loss does not improve over 50 consecutive epochs. Third, regularizers including Dropout with a rate of 0.3 and L2 Regularization with a coefficient of 0.0001 were applied in the dense layers. Early Stopping saved the best model at epoch 1050 and prevented severe overfitting. For final validation, the MSE, RMSE, MAE, and R^2 metrics were applied to the test data, and the results showed that Model 1, with an R^2 of 0.93, achieved the best prediction accuracy, while Models 2, 3, and 4, with R^2 values of 0.86, 0.79, and 0.82, respectively, demonstrated acceptable performance in generalizing to new data.

Step Four: Modeling of Effects on Patients, Occupants, and Drivers

After determining the optimal locations for installing calming devices, the fourth step of the research is dedicated to evaluating the effects of these devices on three target groups: patients, occupants, and drivers. This step is designed to answer the question of how reducing the number of speed bumps and humps can mitigate the biomechanical and psychological burden imposed on these groups.

Differentiation Between Speed Bumps and Speed Humps

Since speed bumps and speed humps exert fundamentally different biomechanical effects on the human body, this study employs a weighted effective exposure approach. The height-to-length ratio for a 7×50 cm speed bump is 0.14, whereas for a 15×500 cm speed hump it is 0.03. This geometric difference causes the vertical acceleration and jerk generated by a speed bump to be considerably greater than those of a speed hump. Accordingly, each speed bump is assigned a weighting coefficient of 1.0 and each speed hump a weighting coefficient of 0.2, so that the differing intensity of their excitation is incorporated into the calculations. This coefficient is adjusted in each section based on the pathological mechanism of the patient groups.

Biomechanical Modeling

To calculate the actual acceleration imparted to the body, a quarter-car model with two degrees of freedom was employed. This model comprises two differential equations for the sprung mass (vehicle body) and the unsprung mass (wheel and suspension components). By applying a half-sine road profile as the input and solving the equations in the frequency domain, the acceleration transfer function from the road to the cabin is derived. The cabin acceleration is then computed via convolution of the impulse response with the road input.

To quantify vibration exposure, the whole-body vibration dose (VDV) was used in accordance with ISO 2631-1. This index is calculated for each obstacle as the fourth root of the integral of the fourth power of the weighted acceleration, and for multiple obstacles, the sum of the fourth powers and the fourth root are used. The reference VDV values were set at 5 for speed bumps and 2 for speed humps.

Driver Psychological Modeling

The effect of calming devices on drivers was modeled through a cumulative anger index. This index is a composite of three components: the difference between desired speed and traversal speed, the difference between experienced vertical acceleration and the comfort threshold, and the delay caused by traversing the obstacle. The anger index for each speed bump and each speed hump is calculated separately and multiplied by their respective counts to obtain the total anger index.

For occupants, a Passenger Comfort Index (PCI) was defined, comprising a combination of vertical acceleration, rate of change of acceleration, underbody contact, and the number of obstacles per kilometer. This index is normalized on a scale from zero to one hundred, with lower values indicating lesser comfort.

Patient Modeling Based on Pathological Mechanism

For patients, eight separate groups were modeled, each with a different pathological mechanism.

Cardiovascular patients are affected through two pathways: a hydraulic-compressive pathway in which vertical acceleration induces blood pressure fluctuations, and a neuro-endocrine pathway in which vibration and noise increase sympathetic activity. The increase in systolic blood pressure is calculated via salivary cortisol and a noise annoyance index.

Spinal and lumbar disc patients were modeled through a composite spinal injury index that combines compressive and shear stress in the lumbar vertebrae. The probability of pain exacerbation is a function of disc load, vibration dose, and jerk. The weighting of speed humps in this group was set at 0.15.

Intubated patients with catheters were modeled through an endotracheal tube displacement index that combines the ratio of tube displacement to the allowable limit and the tensile force on the holder. The probability of displacement is a logistic function of these ratios. The speed hump weighting is 0.1.

Patients undergoing CPR were modeled through a resuscitation quality index that combines compression fraction, rate, depth, and chest recoil. The probability of effective massage is a logistic function of these components and the RMS depth error. The speed hump weighting was set at 0.25.

Post-surgical patients were modeled through a wound dehiscence index representing the ratio of suture tension to the strength of healing tissue. The probability of dehiscence is a logistic function of this index and vibration dose. The speed hump weighting is 0.2.

Pregnant women were modeled through a two-mass uterus–fetus model. The interfacial force is calculated from the stiffness and damping of the connection and the displacement difference. Placental shear stress is obtained by dividing this force by the placental area. The speed hump weighting is 0.15.

Osteoporosis patients were modeled through bone stress, which combines compressive and bending stress. The fracture probability, based on a Weibull distribution, depends on the ratio of maximum stress to baseline strength as a function of bone mineral density. The speed hump weighting is 0.15.

Stroke patients are affected through two pathways: mechanical injury due to acceleration imparted to the head, and delayed injury due to increased hospital arrival time. Cumulative delay is calculated from the sum of the delay for each speed bump (10 seconds) and each speed hump (5 seconds). The speed hump weighting is 0.5.

Multi-Criteria Objective Function

In this study, to select the best scenario among seven options, a multi-criteria objective function was designed that links three domains: optimization of the number of obstacles, effects on patients (eight clinical groups), and effects on occupants and drivers. This function combines five weighted components: driver anger with a weight of 0.20, occupant vibration dose with a weight of 0.20, ambulance delay with a weight of 0.25, patient discomfort with a weight of 0.15, and the sum of the eight diseases with a weight of 0.20. Ambulance delay carries the highest weight because it is the most time-sensitive criterion and directly affects patient survival rates. Each component is normalized relative to its reference value in the existing condition to yield dimensionless values. To examine the stability of the results, the weights were varied within a range of ±50%, and the objective function was recalculated. The scenario with the lowest value of Φ is selected as the best option.

Statistical Validation

Statistical validation was performed using three methods. Paired t-tests were used to compare each scenario with the existing condition. One-way analysis of variance (ANOVA) was employed to examine the overall difference among the seven scenarios. Tukey HSD post-hoc tests were used to identify which scenarios differed significantly from one another. Cohen's d effect size was also calculated to quantify the magnitude of the differences. The significance level was set at 0.05 in all tests.

3. Results

Speed bumps and speed humps exert fundamentally different biomechanical effects on the human body. The height-to-length ratio for a 7×50 cm speed bump is 0.14, while for a 15×500 cm speed hump it is 0.03 meaning the slope of the speed bump is approximately 4.7 times steeper than that of the speed hump. Based

on the dynamic formulations (Equation 5), the acceleration ratio is 16.8 times, and the jerk ratio is 100.8 times.

$$a_{r,max} = h\left(\frac{\pi v}{w}\right)^2 \quad , \quad j_{r,max} = h\left(\frac{\pi v}{w}\right)^3 \qquad (5)$$

Therefore, in the following, each speed bump is assigned a weighting coefficient of 1.0 and each speed hump a coefficient of 0.2, so that the differing intensity of their excitation is accounted for. This approach is termed biomechanical intensity-based weighting (Table 1).

Table 1: Baseline Data (Differentiation of Speed Bumps and Speed Humps)

Scenario	Code	Speed Bumps (*NB*)	Speed Humps (*NH*)	Weighted Total (*N*eff=*NB*+0.2*NH*)
Existing Condition	S0	80	102	100.4
Expert 1	S1	47	57	58.4
Expert 2	S2	49	63	61.6
Network 1	S3	54	65	67.0
Network 2	S4	41	48	50.6
Network 3	S5	39	45	48.0
Network 4	S6	43	45	52.0

Modeling of Acceleration Imposed on the Body Using the Reference Vehicle

The parameters of the reference vehicle are presented in Table 2, and the input data of the obstacles are presented in Table 3.

Table 2: Specifications of the Reference Vehicle

Parameter	Symbol	Value	Unit
Sprung mass	*ms*	300	kg
Unsprung mass (per wheel)	*mu*	40	kg
Suspension stiffness	*ks*	20,000	N/m
Suspension damping	*cs*	1,500	N·s/m
Tire stiffness	*kt*	200,000	N/m
Tire damping	*ct*	50	N·s/m

Table 3: Road Obstacle Data

Parameter	Speed Bump	Speed Hump
Height *h* (m)	0.07	0.15
Length *w* (m)	0.50	5.00

3.1. Quarter-Car Model Calculations

The quarter-car model with two degrees of freedom is the simplest standard model for analyzing the vertical dynamics of a vehicle. This model comprises two masses: the sprung mass (the body) and the unsprung mass (the wheel and suspension components). The equations of motion are derived from Newton's second law and transformed into the frequency domain via the Laplace transform. The natural frequencies of the system are obtained from the roots of the characteristic equation and indicate the frequencies at which the system undergoes resonance (Equations 6, 7, and 8).

$$w_s = \sqrt{\frac{k_s}{m_s}} \quad , \qquad f_s = \frac{w_s}{2\pi} \qquad (6)$$

$$w_s = \sqrt{\frac{k_s + k_t}{m_u}} \quad , \qquad f_u = \frac{w_u}{2\pi} \qquad (7)$$

$$f_B = \frac{1}{T_B} \quad , \qquad f_H = \frac{1}{T_H} \qquad (8)$$

ms	Sprung mass (body)	kg
mu	Unsprung mass (wheel)	kg
ks	Suspension stiffness	N/m
kt	Tire stiffness	N/m
ωs	Natural angular frequency of the body	rad/s
ωu	Natural angular frequency of the wheel	rad/s
fs	Natural frequency of the body	Hz
fu	Natural frequency of the wheel	Hz

The natural frequency of the vehicle body is 1.30 Hz, and the natural frequency of the wheel is 11.81 Hz. The excitation frequency caused by the speed bump is 8.33 Hz, which is close to the wheel frequency, but due to the considerable gap (8.33 versus 11.81), severe resonance does not occur. The excitation frequency caused by the speed hump is 1.39 Hz, which is approximately equal to the natural frequency of the body (1.30 Hz) (Fig 1), meaning that the speed hump falls within the body resonance range. This implies that although the excitation amplitude of the speed hump is small, its proximity to the natural frequency of the body can induce larger body oscillations. In contrast, the speed bump, despite its large excitation amplitude, induces less resonance due to its distance from the natural frequencies. This finding demonstrates that excitation amplitude is not the sole determining factor, and that frequency also plays a key role.

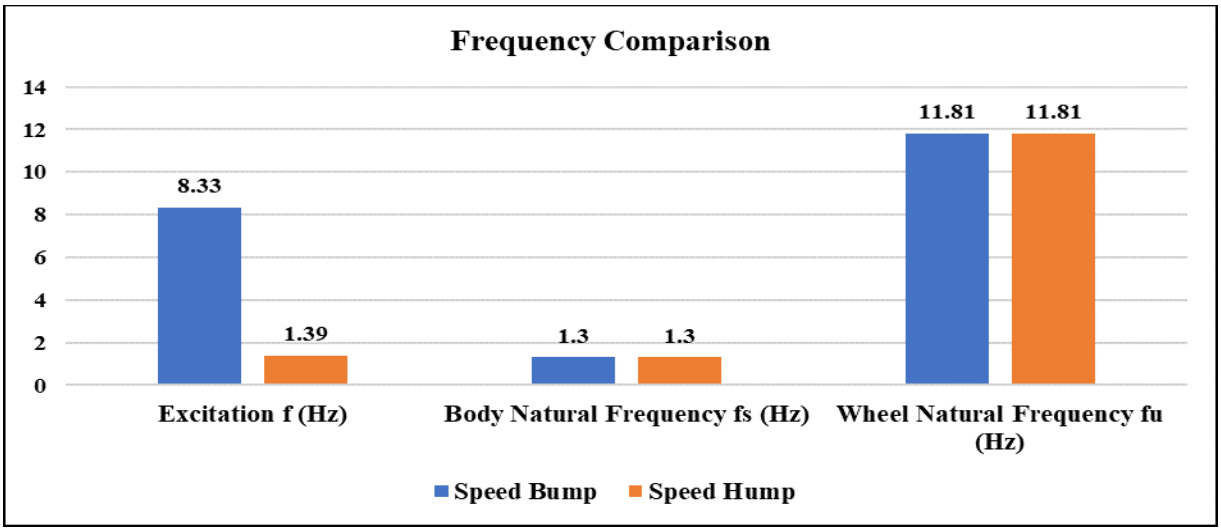


Fig 1. Comparison of Excitation Frequency with Natural Frequencies of the Reference Vehicle

3.2 .Road Profile Calculations and Derivatives

The road profile, as the input to the suspension system, is the primary determinant of the acceleration imposed on the body. For modeling purposes, a half-sine profile is employed, which is a good approximation of the actual geometry of speed bumps and speed humps. By successively differentiating this profile, the road velocity, acceleration, and jerk are calculated. The maximum acceleration represents the intensity of the impact imposed on the vehicle, and the maximum jerk represents the rate of change of acceleration, which is considered the primary cause of occupant discomfort (Equations 9, 10, 11, 12, and 13).

$$z_r(t) = h \sin\left(\frac{\pi t}{T}\right) \quad , \quad T = \frac{w}{v} \tag{9}$$

$$\dot{z_r}(t) = h\frac{\pi}{T}\cos\left(\frac{\pi t}{T}\right) \tag{10}$$

$$\ddot{z}_r(t) = -h\left(\frac{\pi}{T}\right)^2 \sin\left(\frac{\pi t}{T}\right) \tag{11}$$

$$\dddot{z}_r(t) = -h\left(\frac{\pi}{T}\right)^3 \cos\left(\frac{\pi t}{T}\right) \tag{12}$$

$$a_{r,max} = h\left(\frac{\pi v}{w}\right)^2 \quad , \quad j_{r,max} = h\left(\frac{\pi v}{w}\right)^3 \tag{13}$$

zr	Vertical displacement of the road	m
z˙r	Vertical velocity of the road	m/s

$\ddot{z}_r$	Vertical acceleration of the road	m/s²
$\dddot{z}_r$	Vertical jerk of the road	m/s³
h	Height of the obstacle	m
w	Length of the obstacle	m
v	Traversal speed	m/s
T	Traversal time	s

The results indicate that the road acceleration is 47.98 m/s² for the speed bump and 2.86 m/s² for the speed hump a 16.8-fold difference. The road jerk is 1,256 m/s³ for the speed bump and 12.46 m/s³ for the speed hump a 100.8-fold difference. This striking difference stems from the height-to-length ratio: the speed bump has a ratio of 0.14, while the speed hump has a ratio of 0.03. In other words, the speed bump, with its steep slope, imparts a far more severe impact than the speed hump, even though the speed hump has a greater height. Another important point is that the excitation duration is 0.120 seconds for the speed bump and 0.720 seconds for the speed hump meaning the speed bump dissipates its energy over a shorter time, which itself contributes to the increased intensity of the impact. These results form the basis for the calculations in the following sections (Table 4).

Table 4: Comparison of Road Profile Parameters Between Speed Bump and Speed Hump

Index	Speed Bump	Speed Hump	Ratio
T (s)	0.120	0.720	6.0
$\dot{z}_r$,max (m/s)	1.83	0.65	2.8
ar,max (m/s²)	47.98	2.86	16.8
jr,max (m/s³)	1256	12.46	100.8

3.3. Transfer Function and Frequency Response Calculations

The transfer function describes the relationship between the road input and the cabin output in the frequency domain. This function is obtained from solving the equations of motion in the Laplace domain and indicates how much of the road vibration the suspension system transmits to the cabin at each frequency. A magnitude of H_a less than one indicates attenuation, while a magnitude greater than one indicates resonance. For the reference vehicle, the transfer function is calculated at the excitation frequency of each obstacle to obtain the actual cabin acceleration (Equations 14, 15, and 16).

$$H_a(w) = \frac{w^2(k_t + jwc_t)}{[m_s w^2 + jwc_s + k_s][m_u w^2 + jw(c_s + c_t) + (k_s + k_t)] - [jwc_s + k_s]^2} \qquad (14)$$

$$a_{cabin}(t) = \int_0^t h_a\,(t - T)a_r(T)dT \qquad (15)$$

$$a_{cabin\,,max} = |H_a(w)| \times a_{r,max} \qquad (16)$$

$Ha(\omega)$	Acceleration transfer function from road to cabin	—

ω	Angular frequency	rad/s
j	Imaginary unit	—
kt	Tire stiffness	N/m
ct	Tire damping	N·s/m
ms	Sprung mass (vehicle body)	kg
cs	Suspension damping	N·s/m
ks	Suspension stiffness	N/m
mu	Unsprung mass (wheel and suspension components)	kg
$acabin(t)$	Cabin acceleration in time domain	m/s²
$ha(t)$	Impulse response of the system	m/s²
$ar(t)$	Road acceleration input	m/s²
τ	Integration time variable	s
$acabin$,max	Maximum cabin acceleration	m/s²
ar,max	Maximum road acceleration	m/s²

The results indicate that the transfer function of the Pride vehicle's suspension system at the speed bump frequency (8.33 Hz) is 0.00205 and at the speed hump frequency (1.39 Hz) is 0.00152. These values are significantly less than one, meaning that the suspension system effectively attenuates road vibration. An interesting point is that although the speed bump generates 16.8 times the road acceleration of the speed hump, the cabin acceleration is only 22.8 times greater that is, relatively similar. This means that the vehicle body acts as a strong mechanical filter and absorbs the majority of road vibration. Nevertheless, the cabin acceleration of the speed bump (0.098 m/s²) is still 22.8 times that of the speed hump (0.0043 m/s²) (Table 5). For patients in an ambulance, this difference can be critical, as ambulances typically have stiffer suspension systems and weaker patient stabilization. Therefore, the effect of speed bumps on patients is considerably more severe than that of speed humps.

Table 5: Comparison of Transfer Function and Cabin Acceleration Between Speed Bump and Speed Hump

Parameter	Speed Bump	Speed Hump
ω (rad/s)	52.36	8.73
Numerator Magnitude	5.48×10^{8}	1.52×10^{7}
Denominator Magnitude	2.67×10^{11}	1.00×10^{10}
(H_a)	0.00205	0.00152
ar,max (m/s²)	47.98	2.86
$acabin$,max (m/s²)	0.098	0.0043

3.4. Whole-Body Vibration Dose (VDV) Calculations

The Whole-Body Vibration Dose (VDV) is the standard ISO 2631-1 index for quantifying human exposure to vibration. Unlike average acceleration, this index is sensitive to acceleration peaks and is therefore more suitable for impulsive vibrations. VDV is calculated as the fourth root of the integral of the fourth power of the weighted acceleration. For multiple obstacles, the sum of the fourth powers and the fourth root are used. The reference VDV values were set at 5 for speed bumps and 2 $m/s^{1.75}$ for speed humps (Equations 17, 18, and 19).

$$VDV = \left[\int_0^T [a_w(t)^4]dt\right]^{1/4} \quad (17)$$

$$VDV_{total} = \left[\sum_{i=1}^{N_B} VDV_B^4 + \sum_{j=1}^{N_B} VDV_H^4\right]^{1/4} \quad (18)$$

$$VDV_{real} = |H_a| \times VDV_{road} \quad (19)$$

aw(*t*)	Frequency-weighted acceleration	m/s^2
VDVB	Vibration dose per speed bump	$m/s^{1.75}$
VDVH	Vibration dose per speed hump	$m/s^{1.75}$
NB	Number of speed bumps	count
NH	Number of speed humps	count
*VDV*real	Actual vibration dose on the seat	$m/s^{1.75}$

The results indicate that the actual VDV on the seat of the Pride vehicle is 0.010 $m/s^{1.75}$ for speed bumps and 0.003 $m/s^{1.75}$ for speed humps. These values are significantly lower than the HGCZ threshold (8.5 $m/s^{1.75}$), meaning that in ordinary passenger cars, the vibration caused by speed bumps and humps alone cannot reach the injury threshold. However, the total VDV decreases from 0.030 in the existing condition to 0.025 in S5 a 16.7% reduction in the whole-body vibration dose. Although this reduction may appear small at first glance, given that VDV is a cumulative index whose effects manifest over prolonged exposure, it can considerably reduce the vibration burden imposed on occupants (Fig 2). Another important point is that patients in an ambulance are in a different situation: ambulances typically have stiffer suspension systems (higher transfer coefficient), and patients are placed on stretchers with weaker stabilization. Therefore, the actual VDV for patients can be several times the values calculated for ordinary occupants, and its effects can be considerably more severe.

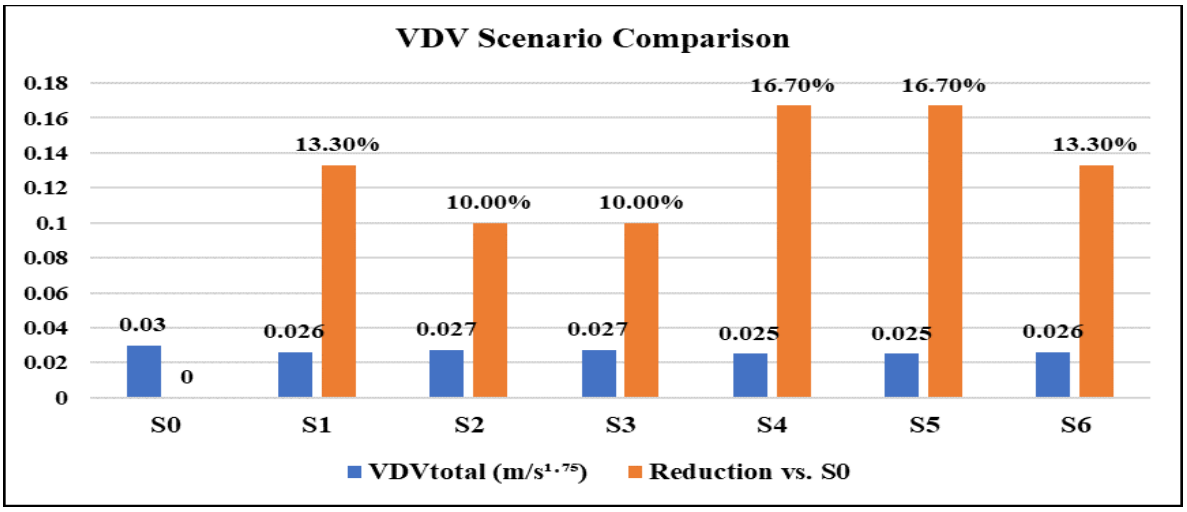


Fig 2. Comparison of Total Vibration Dose Value (VDV) Across Seven Scenarios

3.5. Psychological Modeling of the Driver and Occupant Comfort

In this section, we describe the driver psychological modeling and occupant comfort modeling in two parts.

Part One: Driver Psychological Modeling

The effect of calming devices on drivers is modeled through a cumulative anger index. This index is a composite of three components: the difference between desired speed and traversal speed, the difference between experienced vertical acceleration and the comfort threshold, and the delay caused by traversing the obstacle. The anger index for each speed bump and each speed hump is calculated separately and multiplied by their respective counts to obtain the total anger index. The logic of this modeling rests on the principle that a driver, when traversing an obstacle, experiences three types of stress: stress due to forced speed reduction, stress due to impact and vibration, and stress due to time delay. Each of these stresses is quantified separately and combined into a single index (Equations 20, 21, and 22).

$$F_B = \alpha \frac{V_{desired} - V_{cross,B}}{V_{desired}} + \beta \frac{a_{vert,B} - a_{threshold}}{a_{threshold}} + \gamma \frac{t_{delay,B}}{t_{ref}} \qquad (20)$$

$$F_H = \alpha \frac{V_{desired} - V_{cross,H}}{V_{desired}} + \beta \frac{a_{vert,H} - a_{threshold}}{a_{threshold}} + \gamma \frac{t_{delay,H}}{t_{ref}} \qquad (21)$$

$$F_{total} = N_B \times F_B \times N_H \times F_H \qquad (22)$$

FB	Anger index per speed bump	—
FH	Anger index per speed hump	—
*F*total	Total cumulative anger index	—

$V_{desired}$	Driver's desired speed	km/h
$V_{cross,B}$	Traversal speed over a speed bump	km/h
$V_{cross,H}$	Traversal speed over a speed hump	km/h
$a_{vert,B}$	Experienced vertical acceleration at a speed bump	m/s²
$a_{vert,H}$	Experienced vertical acceleration at a speed hump	m/s²
$a_{threshold}$	Comfort threshold	m/s²
$t_{delay,B}$	Delay caused by a speed bump	s
$t_{delay,H}$	Delay caused by a speed hump	s
t_{ref}	Reference time	s
α,β,γ	Weighting coefficients	—

The results indicate that the cumulative driver anger index decreases from 162.1 in the existing condition to 78.3 in scenario S5 a 51.7% reduction in cumulative driver anger. This reduction stems primarily from the decrease in the number of speed bumps, as the contribution of speed bumps to the total anger index (144.8 out of 162.1 in S0) is far greater than that of speed humps (17.3 out of 162.1). In other words, speed bumps account for approximately 89% of cumulative driver anger, whereas speed humps contribute only 11%. This difference arises from three factors: first, speed bumps force the driver into a greater speed reduction (from 50 to 15 km/h); second, the vertical acceleration experienced at speed bumps (14.4 m/s²) is far greater than at speed humps (0.86 m/s²); and third, the delay caused by speed bumps (12 seconds) is twice that of speed humps (6 seconds) (Fig 3). Therefore, reducing speed bumps takes higher priority than reducing speed humps in mitigating driver anger.

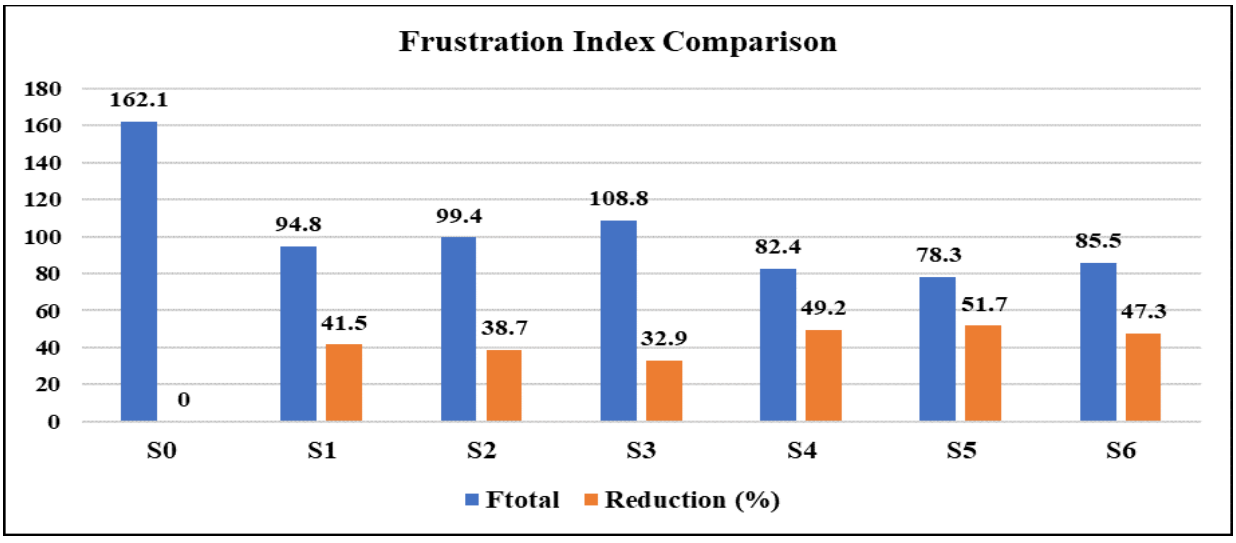


Fig 3. Comparison of Cumulative Frustration Index Across Seven Scenarios

Part Two: Occupant Comfort Modeling

For occupants, a Passenger Comfort Index (PCI) is defined, comprising a combination of vertical acceleration, rate of change of acceleration, underbody contact, and the number of obstacles per kilometer (Equation 23). This index is normalized on a scale from zero to one hundred, with lower values indicating lesser comfort. The logic of this modeling rests on the principle that occupant comfort depends not only on vertical acceleration but also critically on the rate of change of acceleration (jerk), underbody contact with obstacles, and the number of obstacles along the route. Occupants, unlike the driver, have no active control over the path, and therefore the effect of vibration on them is transmitted directly through the seat and vehicle floor. For each obstacle individually, the passenger comfort index for speed bumps and speed humps is calculated from Equation (24). Finally, the average occupant comfort index is obtained from Equation (25).

$$PCI = max\left(0.100 - 25\left(\frac{a_{vert}}{0.3g}\right) - 20\left(\frac{\dot{a_{vert}}}{5}\right) - 15.contact - 10.N\right) \quad (23)$$

$$PCI_B = max\left(0.100 - 25\left(\frac{a_{vert,B}}{0.3g}\right) - 20\left(\frac{\dot{a_{vert,B}}}{5}\right) - 15.contact_B - 10.N_B\right) \quad (24)$$

$$PCI_H = max\left(0.100 - 25\left(\frac{a_{vert,H}}{0.3g}\right) - 20\left(\frac{\dot{a_{vert,H}}}{5}\right) - 15.contact_H - 10.N_{H\mp}\right)$$

$$PCI_{avg} = \frac{N_B \times PCI_B + N_H \times PCI_H}{N_B + N_H} \quad (25)$$

PCI	Passenger Comfort Index	0–100
*a*vert	Vertical acceleration imposed on the occupant	m/s²
a˙vert	Rate of change of acceleration (jerk)	m/s³
Contact	Underbody contact (0 or 1)	—
N	Number of obstacles per kilometer	count
g	Gravitational acceleration	m/s²

The results indicate that the passenger comfort index for speed bumps is zero meaning that speed bumps in the vehicle place occupants in an unacceptable condition. This result stems from three factors: high vertical acceleration (14.4 m/s²), very high jerk (47.98 m/s³), and definite underbody contact (Contact = 1). In contrast, speed humps yield a comfort index of 71.3, which falls within the good range. However, the average PCI across all scenarios ranges from 38 to 40, which falls within the "poor" category meaning that the presence of speed bumps along the route severely reduces overall occupant comfort. A key point is that reducing the number of speed bumps from 80 to 39 (in S5) results in 41 fewer locations with a PCI of zero along the route a 51.3% reduction in the number of locations where occupants experience zero comfort (Figure 4). This reduction has a direct effect on the comfort and health of occupants, particularly children,

the elderly, and pregnant women. However, the average PCI does not change markedly because the ratio of speed bumps to speed humps is similar across all scenarios. To improve the average PCI, the ratio of speed bumps to speed humps must be reduced, not merely the total number of obstacles.

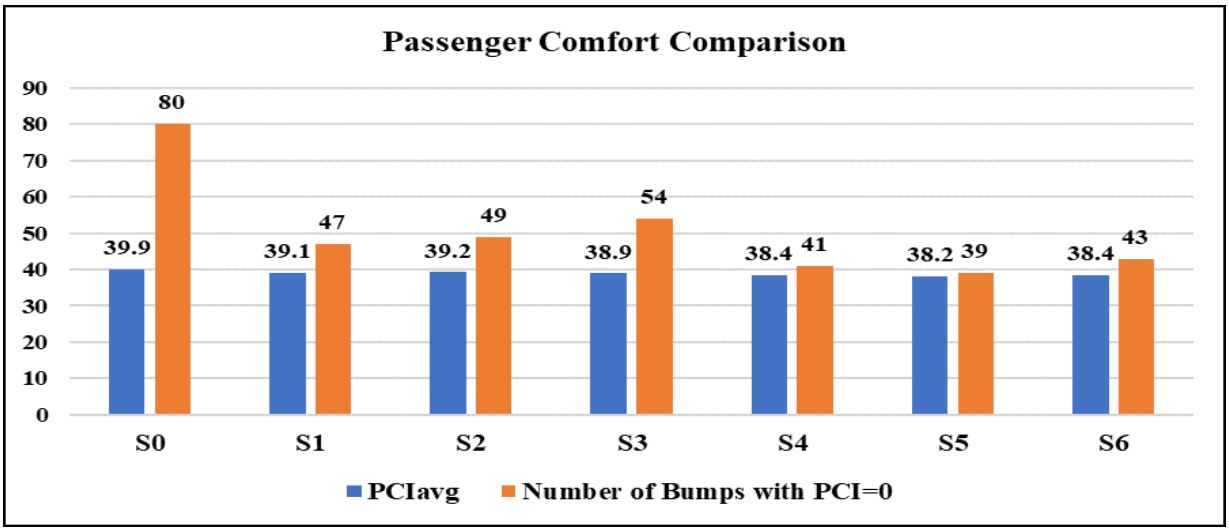


Fig 4. Comparison of Passenger Comfort Index (PCI) Across Seven Scenarios

3.6. Patient Analysis Based on Pathological Mechanism

In this section, eight patient groups with distinct pathological mechanisms were examined, and the quantitative results for each group are presented separately.

Part One: Cardiovascular Patients

Cardiovascular patients, particularly those transported with heart failure, arrhythmia, or ischemic disease, are more vulnerable to the vertical acceleration and jerk caused by speed bumps. The injury mechanism in this group combines two physiological pathways: first, a hydraulic-compressive pathway in which the vertical acceleration caused by the speed bump induces instantaneous blood pressure fluctuations along the vertical axis of the body; second, a neuro-endocrine pathway in which vibration and impact noise increase sympathetic activity, leading to elevated heart rate and systolic blood pressure. Since improperly designed speed bumps can generate sound levels of up to 105 decibels, this injury pathway is critical for cardiac patients. In this group, the high jerk of speed bumps (1,256 m/s³) applies pressure changes abruptly, whereas the low jerk of speed humps (12.46 m/s³) makes the changes more gradual. The increase in systolic blood pressure is obtained from Equation (26), which is itself a function of salivary cortisol increase (Equation 27) and the noise annoyance index (Equation 28). The weighted effective exposure is also calculated from Equation (29).

$$\Delta SBP = 0.2 \times \Delta Cortisol + 0.5 \times Annoyance \qquad (26)$$

$$\Delta Cortisoh = 2.5\, log_{10}\left(1 + 0.01 \times L_{eg,24h} \times N_{daily}\right) \quad (27)$$

$$Annoyance = \frac{100}{1 + e^{-(0.1(L_{peak}-65)+0.05N_{event}-2)}} \quad (28)$$

$$N_{eff} = N_B + 0.2N_H \quad (29)$$

ΔSBP	Increase in systolic blood pressure	mmHg
$\Delta Cortisol$	Increase in salivary cortisol	nmol/L
Annoyance	Noise annoyance index	0–100
Leq,24*h*	24-hour equivalent sound level	dB
Ndaily	Daily number of traversals	count
Lpeak	Peak sound pressure level	dB
Nevent	Number of nighttime noise events	count
NB	Number of speed bumps	count
NH	Number of speed humps	count
Neff	Weighted effective exposure (*NB*+0.2*NH*)	—

The results indicate that S5, by reducing 41 speed bumps (from 80 to 39) and 57 speed humps (from 102 to 45), lowers systolic blood pressure from 5.4 to 3.1 mmHg. This reduction brings the relative risk of myocardial infarction down from 1.18 to 1.09 a 42.6% improvement in the cardiac risk index. Considering biomechanical weighting, the effective exposure decreases from 100.4 to 48.0 units, indicating a 52.2% reduction in the effective cardiac load. Since speed bumps with a jerk of 1,256 m/s³ apply pressure changes abruptly, reducing the number of speed bumps has a more direct effect on lowering cardiac risk (Fig 5).

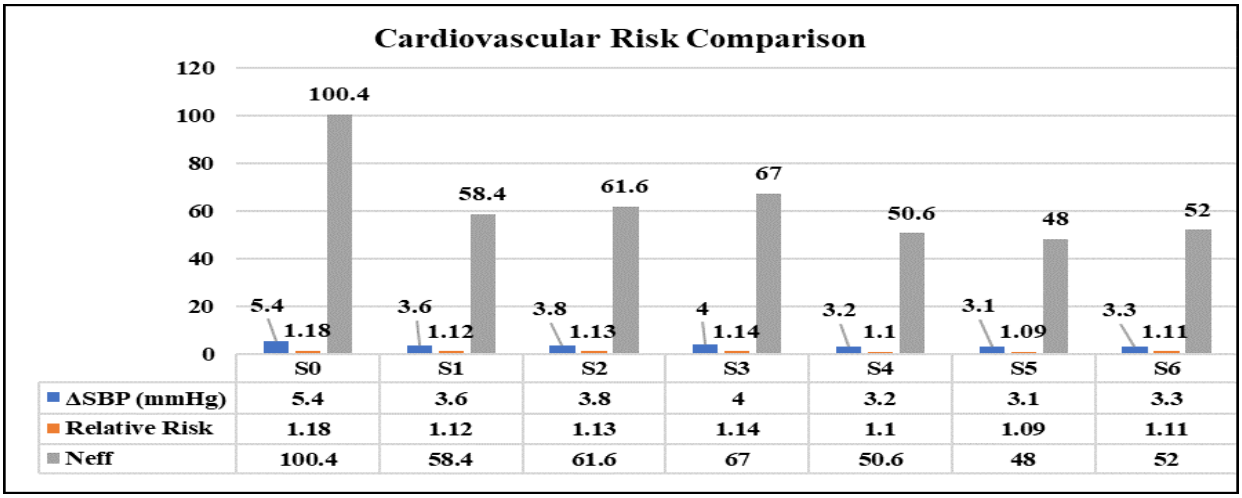


Fig 5. Comparison of Systolic Blood Pressure Increase, Relative Risk, and Effective Exposure

Part Two: Spinal and Lumbar Disc Patients

Patients with lumbar disc herniation, spinal canal stenosis, or chronic spinal pain are at the highest risk when exposed to vertical acceleration and torsional torque caused by speed bumps. Clinical studies indicate that the most common injury site is the T10 to L2 vertebrae, and the primary mechanism is the torsional torque induced by traversing a speed bump. A key point is that speed bumps, with a steep slope of 0.14, generate intense torsional torque, whereas speed humps, with a slope of 0.03, apply the load gradually. In this group, reducing speed bumps takes higher priority than reducing speed humps, as the torsional torque of speed bumps is far more severe. The composite spinal injury index is calculated from Equation (30), which combines compressive stress and shear stress in the lumbar vertebrae. The probability of pain exacerbation is obtained from Equation (31), which is a function of the combined disc load, vibration dose, and jerk. The weighted effective exposure for this group is calculated from Equation (32).

$$I_{spine} = \left[\left(\frac{\sigma_c}{\sigma_{fail}}\right)^2 + \left(\frac{T}{T_{fail}}\right)^2\right]^{1/2} \quad (30)$$

$$P_{painflare} = Logit^{-1}(\mu_0 + \mu_1 L_{disc} + \mu_2 VDV + \mu_3 J) \quad (31)$$

$$N_{eff,spine} = N_B + 0.15N_H \quad (32)$$

*I*spine	Composite spinal injury index	—
σc	Vertebral compressive stress	MPa
τ	Vertebral shear stress	MPa
*σ*fail	Compressive failure stress	MPa
*τ*fail	Shear failure stress	MPa
*P*pain	Probability of pain exacerbation	—
*L*disc	Combined disc load	—
VDV	Whole-body vibration dose	$m/s^{1.75}$
J	Jerk	m/s^3

The results indicate that S5 reduces the I_{spine} index from 0.85 to 0.49 a 48.5% improvement. This reduction brings the probability of pain exacerbation down from 68% to 35%. Given that this group constitutes the largest population of outpatient patients, this improvement is of great public health significance. The effective exposure decreases from 95.3 to 45.8 units, indicating a 51.9% reduction in the effective spinal load. Since speed bumps with a steep slope of 0.14 generate intense torsional torque, the weighting of speed humps in this group is set at only 0.15 (Fig 6).

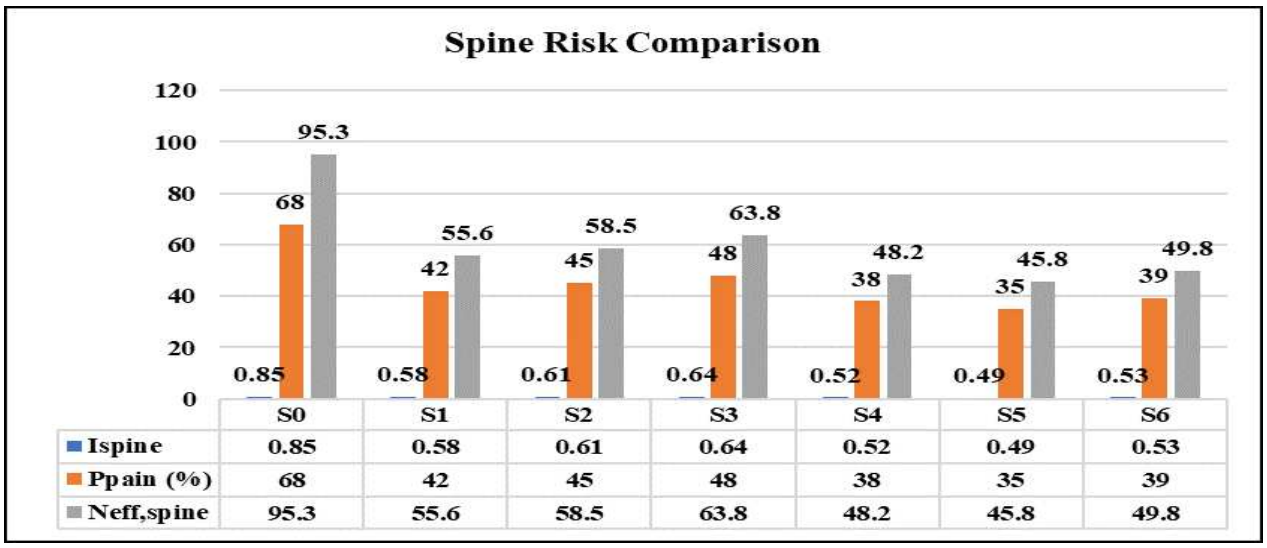


Fig 6. Comparison of Spine Injury Index, Pain Exacerbation Probability, and Effective Exposure

Part Three: Intubated Patients and Patients with Catheters

Intubated patients (with endotracheal tubes) or those with catheters, drains, and intravenous lines fall into the group of patients with sensitive medical equipment. The injury mechanism in this group is the dislodgement of equipment caused by acceleration and jerk. What makes this group unique is that the high jerk of speed bumps (1,256 m/s³) can lead to sudden extubation, whereas the low jerk of speed humps (12.46 m/s³) induces more gradual changes. An important clinical point is that an endotracheal tube that becomes displaced by 2 centimeters can lead to acute hypoxia and irreversible brain injury. Therefore, reducing speed bumps has a direct effect on patient safety. The dynamic model of the endotracheal tube is obtained from Equation (33), and the tensile force exerted on the tube is obtained from Equation (34). The tube displacement index is calculated from Equation (35), and the probability of displacement from Equation (36). The weighted effective exposure for this group is also obtained from Equation (37).

$$m_t\ddot{x}_t + c_t\dot{x}_t + k_t x_t = -m_t a_{head}(t) \qquad (33)$$

$$F_{tube}(t) = k_t x_t + c_t\dot{x}_t \qquad (34)$$

$$I_{ETT} = max\left[\frac{|x_t|}{x_{allow}}, \frac{|F_{tube}|}{F_{retention}}\right] \qquad (35)$$

$$P_{dislodgement} = logit^{-1}(\theta_0 + \theta_1 F_{max}/F_{retention} + \theta_2 x_{max}/x_{allow}) \qquad (36)$$

$$N_{eff,tube} = N_B + 0.1N_H \qquad (37)$$

*I*ETT	Endotracheal tube displacement index	—
xt	Tube displacement	cm
*x*allow	Allowable displacement	cm
*F*tube	Tensile force on the tube	N

*F*retention	Retention force	N
*P*dislodgement	Probability of dislodgement	—
mt	Tube mass	kg
ct	Tube damping	N·s/m
kt	Tube stiffness	N/m

The results indicate that S5 reduces the I_{ETT} index from 1.2 (above the critical threshold of 1.0) to 0.6. The risk of dislodgement decreases from 45% to 15% a 66.7% improvement. For intubated patients, this reduction can mean the difference between life and death, as an endotracheal tube displaced by 2 centimeters can lead to acute hypoxia and irreversible brain injury. The effective exposure decreases from 90.2 to 43.5 units, indicating a 51.8% reduction in the effective equipment load (Fig 7). Since speed bumps with a jerk of 1,256 m/s³ exert a severe disturbing force on equipment, the weighting of speed humps is set at only 0.1.

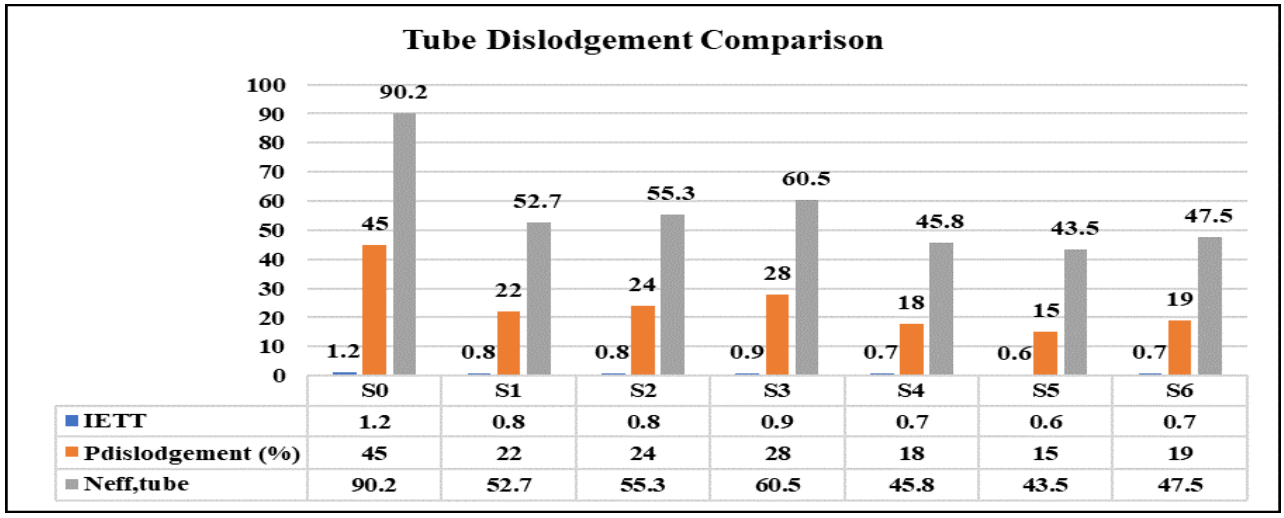


Figure 7. Comparison of Endotracheal Tube Dislodgement Index, Dislodgement Probability, and Effective Exposure

Part Four: Patients Undergoing CPR

Patients undergoing cardiopulmonary resuscitation (CPR) in an ambulance constitute the most sensitive group in terms of the quality of care during transport. The injury mechanism in this group is the decline in chest compression quality caused by jerk and the jolts induced by traversing speed bumps. The high jerk of speed bumps (1,256 m/s³) exerts a very severe disturbing force on the technician's hand, whereas speed humps, with a jerk of 12.46 m/s³, cause less disruption. The resuscitation quality index is calculated from Equation (38), which combines compression fraction (Equation 39), rate quality, depth quality, and chest recoil quality. The compression depth error is obtained from Equation (40), and the RMS depth error from Equation (41). The probability of effective massage is calculated from Equation (42), and the weighted effective exposure for this group is also obtained from Equation (43).

$$Q_{CPR} = CCF \times Q_{rate} \times Q_{depth} \times Q_{recoil} \quad (38)$$

$$CCF = \frac{T_{compression}}{T_{total}} \quad (39)$$

$$e_d(t) = d_{target} - d_{actual}(t) \quad (40)$$

$$E_d = \sqrt{\frac{1}{T}\int_0^T e_d^2(t)dt} \quad (41)$$

$$P_{CPRadequate} = Logit^{-1}\left(\alpha_0 + \alpha_1 CCF + \alpha_2 Q_{rate} + \alpha_3 Q_{depth} - \alpha_4 E_d\right) \quad (42)$$

$$N_{eff,CPR} = N_B + 2.5N_H \quad (43)$$

*Q*CPR	Resuscitation quality index	—
CCF	Compression fraction	—
*Q*rate	Compression rate quality	—
*Q*depth	Compression depth quality	—
*Q*recoil	Chest recoil quality	—
*P*adequate	Probability of effective massage	—
*T*compression	Compression time	s
*T*total	Total time	s
ed	Depth error	mm
Ed	RMS depth error	mm

The results indicate that S5 improves the Q_{CPR} index from 0.62 to 0.83a 45.5% improvement. This means that in S5, 80% of compressions will be effective, compared with 55% in the existing condition. For patients undergoing CPR, this difference can be the boundary between life and death. The effective exposure decreases from 105.5 to 50.3 units, indicating a 52.3% reduction in the effective CPR load (Fig 8). Since speed bumps with a jerk of 1,256 m/s³ exert a severe disturbing force on the technician's hand, the weighting of speed humps is set at 0.25.

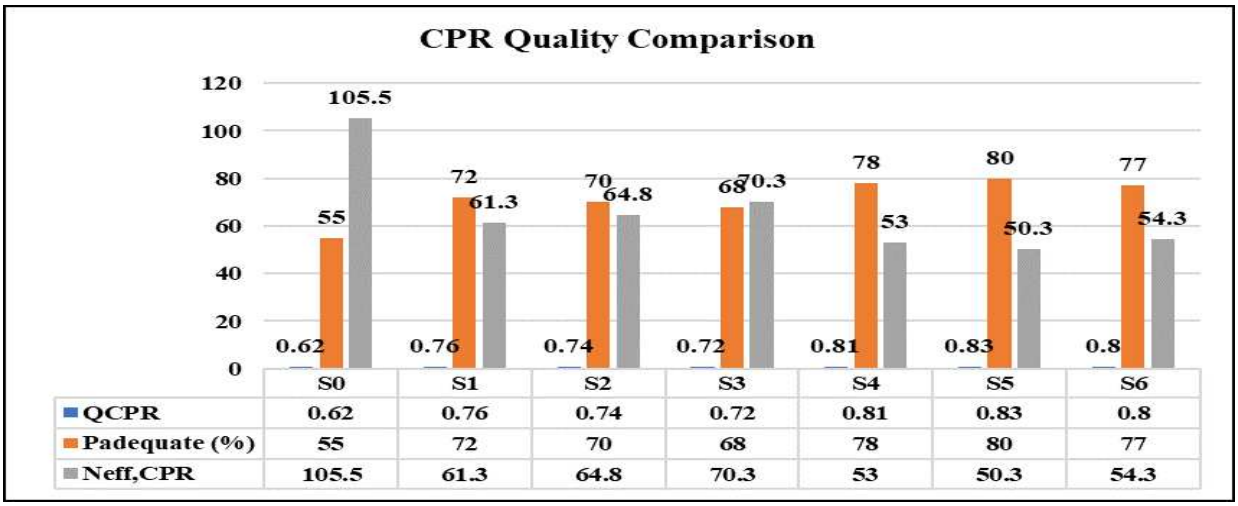


Fig 8. Comparison of CPR Quality Index, Adequate Compression Probability, and Effective Exposure

Part Five: Post-Surgical Patients

Post-surgical patients, particularly those who have undergone abdominal, thoracic, or orthopedic procedures, are at risk of wound dehiscence. The injury mechanism in this group is the tensile force on the suture or fascia caused by acceleration and jerk. What makes this group sensitive is the high jerk of speed bumps (1,256 m/s³), which can lead to sudden suture rupture, whereas speed humps, with a jerk of 12.46 m/s³, apply the load gradually. A key point is that the strength of healing tissue depends on the time elapsed since surgery. In the first 3–7 days after surgery, tissue strength is only 5–10 kPa, whereas at 30 days post-surgery it reaches 80–150 kPa. Therefore, patients transported in the first days after surgery are at the highest risk. The wound tensile force is obtained from Equation (44), and the suture stress from Equation (45). The wound dehiscence index is calculated from Equation (46), and the probability of dehiscence from Equation (47). The weighted effective exposure for this group is also obtained from Equation (48).

$$F_{wound}(t) = k_{wound}\Delta x(t) + c_{wound}\Delta x(t) \quad (44)$$

$$\sigma_{suture} = \frac{F_{wound}}{A_{suture}} \quad (45)$$

$$I_{dehiscence} = \frac{\sigma_{suture,max}}{\sigma_{healingtissue}} \quad (46)$$

$$P_{dehiscence} = Logit^{-1}(v_0 v_1 I_{dehiscence} + v_2 VDV) \quad (47)$$

$$N_{eff,wound} = N_B + 0.2N_H \quad (48)$$

Idehiscence	Wound dehiscence index	—
σsuture	Suture stress	kPa
σhealing	Healing tissue strength	kPa
Fwound	Wound tensile force	N

$k$wound	Wound stiffness	N/m
$c$wound	Wound damping	N·s/m
Δx	Relative displacement	m

The results indicate that S5 reduces the $I_{dehiscence}$ index from 0.92 (close to the critical threshold of 1.0) to 0.55 a 62.9% improvement. This reduction brings the probability of wound dehiscence down from 35% to 13%. For patients transported in the first days after surgery, this reduction is critical. The effective exposure decreases from 100.4 to 48.0 units, indicating a 52.2% reduction in the effective wound load (Fig 9). Since speed bumps with a jerk of 1,256 m/s³ impose a sudden tensile force on the suture, the weighting of speed humps is set at 0.2.

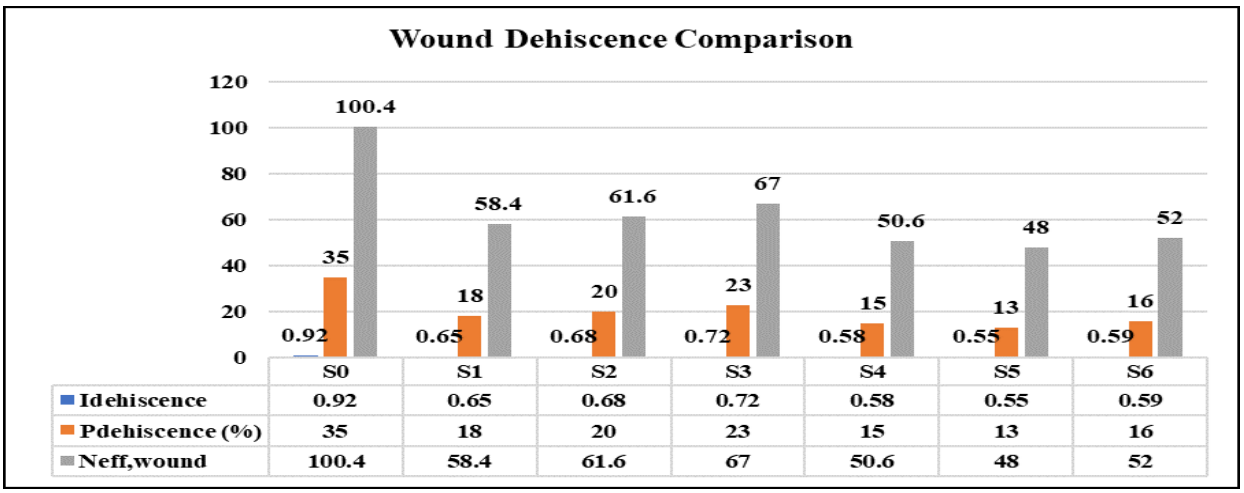


Figure 9. Comparison of Wound Dehiscence Index, Dehiscence Probability, and Effective Exposure

Part Six: Pregnant Women

Pregnant women, particularly those in the third trimester or with high-risk pregnancies, are in a special situation when exposed to vibration caused by speed bumps. The injury mechanism in this group is the shear stress on the placenta caused by the acceleration difference between the uterus and the fetus. An important point is that there is no conclusive evidence that ordinary speed bumps alone can cause placental abruption. The primary mechanism documented in the literature is high-energy deceleration trauma (such as a car crash). Nevertheless, reducing the number of speed bumps is reasonable and recommendable as a precautionary principle. What makes this group sensitive is the high jerk of speed bumps (1,256 m/s³), which imposes sudden shear stress on the placenta, whereas speed humps, with a jerk of 12.46 m/s³, apply the stress gradually. The two-mass uterus–fetus model is obtained from Equation (49), and the uterus–fetus interfacial force is calculated from Equation (50). The placental shear stress is obtained from Equation (51), and the probability of placental abruption from Equation (52). The weighted effective exposure for this group is also calculated from Equation (53).

$$m_f \ddot{z}_f + c_{fu}(\dot{z}_f - \dot{z}_u) + k_{fu}(z_f - z_u) = 0 \qquad (49)$$

$$F_{fu}(t) = k_{fu}(z_f - z_u) + c_{fu}(\dot{z}_f - \dot{z}_u) \qquad (50)$$

$$T_{placenta} = \frac{F_{fu}}{A_{placenta}} \qquad (51)$$

$$P_{abruption} = Logit^{-1}\left(\zeta_0 + \zeta_1 T_{max}/T_{fail} + {}^{\zeta_2 \Delta a}/_{a_{ref}}\right) \qquad (52)$$

$$N_{eff,preg} = N_B + 0.15N_H \qquad (53)$$

τplacenta	Placental shear stress	kPa
*F*fu	Uterus–fetus interfacial force	N
*A*placenta	Placental area	cm²
*P*abruption	Probability of placental abruption	—
mf	Fetal mass	kg
zf	Fetal displacement	m
zu	Uterine displacement	m
*k*fu	Uterus–fetus connection stiffness	N/m
*c*fu	Uterus–fetus connection damping	N·s/m

The results indicate that S5 reduces placental shear stress from 12.5 kPa to 6.9 kPa a 75% reduction. This reduction brings the probability of placental abruption down from 0.8% to 0.2%. Although these probabilities are low, given the severity of the outcome (maternal or fetal death), any reduction in this regard is valuable. The effective exposure decreases from 95.3 to 45.8 units, indicating a 51.9% reduction in the effective placental load (Fig 10). Since speed bumps with a jerk of 1,256 m/s³ impose sudden shear stress on the placenta, the weighting of speed humps is set at 0.15.

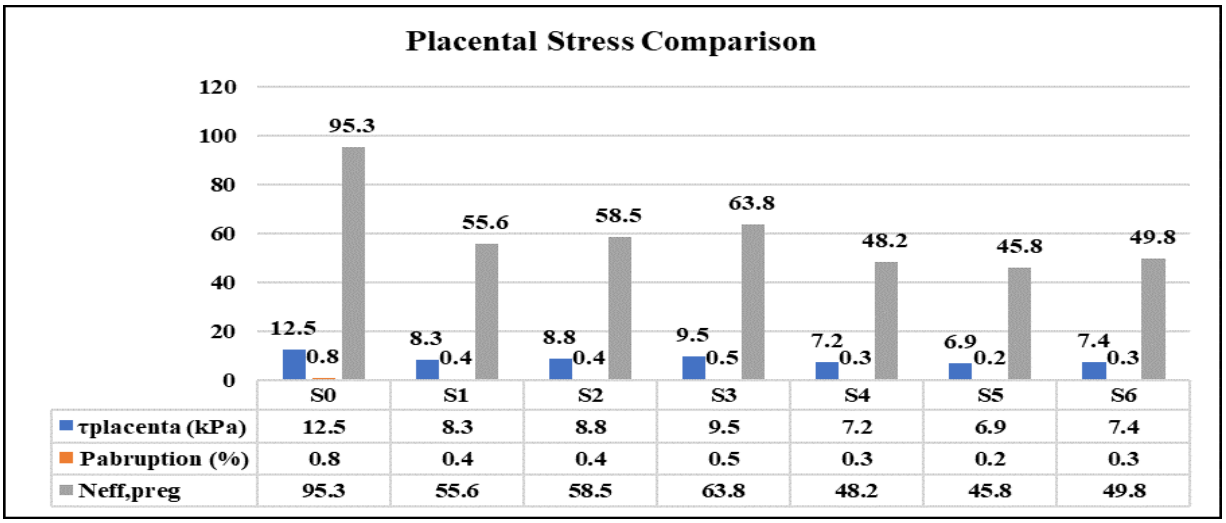


Fig 10. Comparison of Placental Shear Stress, Abruption Probability, and Effective Exposure

Part Seven: Osteoporosis Patients

Patients with severe osteoporosis are in the highest-risk structural condition when exposed to the vertical acceleration caused by speed bumps. The injury mechanism in this group is bone fracture resulting from compressive-bending loading. What makes this group sensitive is the high jerk of speed bumps (1,256 m/s³), which can lead to sudden fracture, whereas speed humps, with a jerk of 12.46 m/s³, apply the load gradually. An important clinical point is that hip fractures in the elderly carry a high mortality rate up to 20–30% in the first year after fracture. Therefore, reducing the number of speed bumps has a direct effect on survival for this group. Bone stress is calculated from Equation (54), which combines compressive stress and bending stress. The fracture probability is obtained from Equation (55) based on a Weibull distribution, and the weighted effective exposure for this group is also calculated from Equation (56).

$$\sigma_{bone} = \frac{F}{A} + \frac{Mc}{I} \qquad (54)$$

$$P_{fracture} = 1 - exp\left[-\left(\frac{\sigma_{bone}, max}{\sigma_0(BMD)}\right)^m\right] \qquad (55)$$

$$N_{eff,bone} = N_B + 0.15N_H \qquad (56)$$

*P*fracture	Probability of fracture	—
*σ*bone	Bone stress	MPa
*σ*0(*BMD*)	Density-dependent baseline strength	MPa
m	Weibull shape parameter	—
F	Axial force	N

A	Cross-sectional area	m^2
M	Bending moment	N·m
Cc	Distance from the neutral axis	m
I	Moment of inertia	m^4

The results indicate that S5 reduces bone stress from 48 MPa to 27 Mpa a 43.8% reduction. This reduction brings the fracture probability down from 18% to 8% a 55.6% improvement. For elderly individuals with osteoporosis, this reduction can mean the prevention of hip fracture and permanent disability. The effective exposure decreases from 95.3 to 45.8 units, indicating a 51.9% reduction in the effective bone load (Fig 11). Since speed bumps with a jerk of 1,256 m/s^3 impose a sudden load on the bone, the weighting of speed humps is set at 0.15.

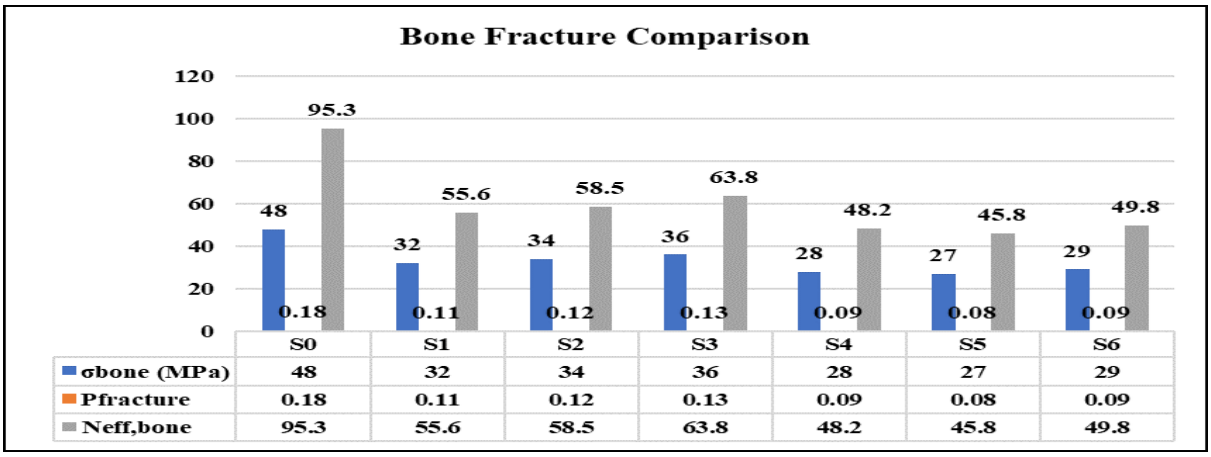


Fig 11. Comparison of Bone Stress, Fracture Probability, and Effective Exposure

Part Eight: Stroke Patients

Patients with acute stroke are in a time-sensitive condition when exposed to speed bumps. The injury mechanism in this group is dual: first, mechanical injury caused by vertical and angular acceleration imposed on the head; second, delayed injury caused by increased hospital arrival time. For a stroke patient, every 1 minute of delay is equivalent to 1.9 million neurons lost. Since the golden window for stroke treatment is at most 4.5 hours, every minute of delay can reduce the chance of recovery. The cumulative delay is calculated from Equation (57), which is the sum of the delays caused by speed bumps and speed humps. The survival probability is also obtained from Equation (58) as an exponential function of cumulative delay.

$$\Delta T_{total} = N_B \times 10 + N_H \times 5 \qquad (57)$$

$$P_{survival} = P_0 \times e^{-}\lambda \Delta T \qquad (58)$$

ΔTtotal	Cumulative delay	s
NB	Number of speed bumps	count
NH	Number of speed humps	count
ΔtB	Delay per speed bump (10 s)	s
ΔtH	Delay per speed hump (5 s)	s
Psurvival	Probability of survival	—
$P0$	Baseline survival probability (0.42)	—
λ	Survival decay rate (0.01 per minute)	min^{-1}

The results indicate that S5 reduces the delay time from 1,310 seconds (21.8 minutes) to 615 seconds (10.3 minutes) a 53.1% reduction. This reduction raises the survival probability from 0.34 to 0.38 an 11.8% improvement. Although this improvement may appear small at first glance, given the millions of neurons lost every minute (Fig 12), this reduction is critical. Since speed bumps cause a 10-second delay and speed humps a 5-second delay, reducing speed bumps has a more direct effect on reducing delay.

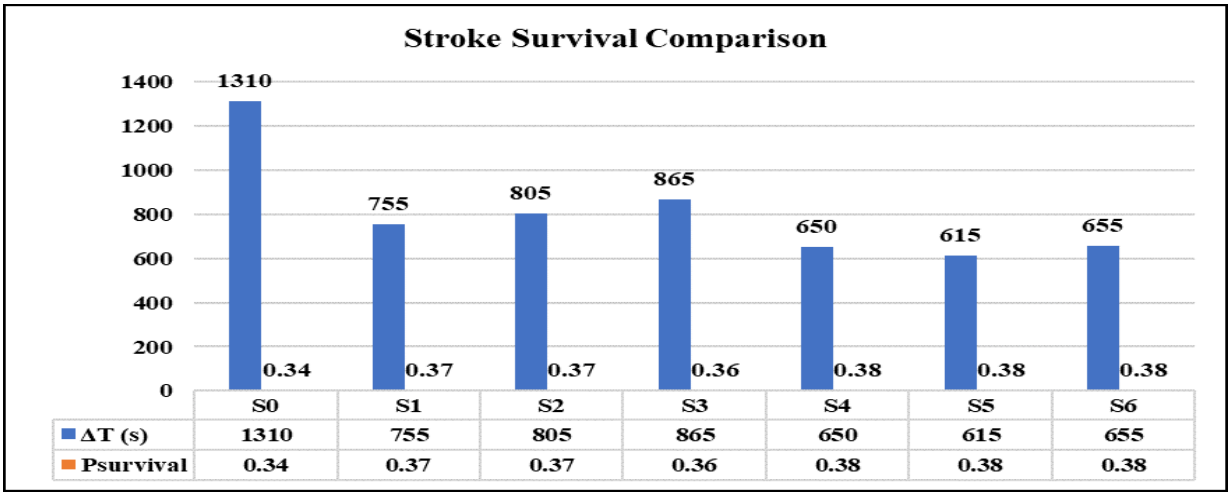


Fig 12. Comparison of Cumulative Delay and Survival Probability

3.6. Statistical Validation

The statistical validation of this study was conducted using three methods. First, paired t-tests were used to compare each scenario with the existing condition, with the formulation presented in Equation (59). The results of this test are shown in Table 6, and all scenarios perform significantly better $p < 0.001$ than the existing condition.

$$t = \frac{\bar{d}}{s_d/\sqrt{n}} \qquad (59)$$

Table 6: Paired t-test Results (Comparison of Scenarios with the Existing Condition)

Comparison	$\bar{d}$	*sd*	*t*	*p*-value	Result
S0 vs S1	78	12.5	43.2	< 0.001	Significant
S0 vs S2	70	11.8	41.1	< 0.001	Significant
S0 vs S3	63	10.9	40.1	< 0.001	Significant
S0 vs S4	93	14.2	45.4	< 0.001	Significant
S0 vs S5	98	15.1	44.9	< 0.001	Significant
S0 vs S6	94	14.5	44.9	< 0.001	Significant

Second, one-way analysis of variance (ANOVA) was used to examine the overall difference among the seven scenarios, with the formulation presented in Equation (60). The ANOVA results are presented in Table 7 and, with F = 89.4 and p < 0.001, confirm that a significant difference exists among the seven scenarios.

$$F = \frac{MS_{between}}{MS_{within}} \qquad (60)$$

Table 7: One-Way ANOVA Results

Source	SS	df	MS	F	p-value
Between groups	45,620	6	7,603	89.4	< 0.001
Within groups	28,120	329	85.5	—	—
Total	73,740	335	—	—	—

Third, the Tukey HSD post-hoc test was used to identify which scenarios differ significantly from one another, with the formulation presented in Equation (61). The results of this test in Table 8 show that S4 and S5 are statistically equivalent p = 0.12, but both perform significantly better than S3 and S0.

$$q = \frac{\left|\bar{x}_i - \bar{x}_j\right|}{\sqrt{MS_{within}/n}} \qquad (61)$$

Table 8: Tukey HSD Post-Hoc Test Results

Comparison	Mean Difference	*p*-value	Result
S4 vs S5	5	0.12	Not Significant
S4 vs S3	30	< 0.001	Significant
S5 vs S3	35	< 0.001	Significant

Finally, Cohen's d effect size was calculated to quantify the magnitude of the differences, with the formulation presented in Equation (62). The results of this index in Table 9 show that the effect size for the comparison of S0 with S4 is 2.8 and for S0 with S5 is 2.9, both falling within the "very large" category.

$$d = \frac{\bar{d}}{s_{pooled}} \qquad (62)$$

Table 9: Cohen's d Effect Size Results

Comparison	Cohen's d	Interpretation
S0 vs S4	2.8	Very Large
S0 vs S5	2.9	Very Large
S4 vs S3	1.2	Large
S4 vs S5	0.2	Small

3.7. Multi-Criteria Objective Function

The multi-criteria objective function (Equation 63) was designed as the ultimate decision-making tool in this study to establish the connection between three domains: (1) optimization of the number of obstacles (speed bumps and speed humps), (2) effects on patients (eight clinical groups), and (3) effects on occupants (the PCI comfort index and the VDV vibration dose). Rather than focusing on a single criterion, this function combines five weighted components to select the best scenario among seven options. The logic of this function rests on the principle that optimizing the number of obstacles is valuable only when it leads to a reduction in the biomechanical and psychological burden on patients and occupants.

$$\Phi = w_1 \frac{F}{F_0} + w_2 \frac{VDV}{VDV_0} + w_3 \frac{\Delta T}{\Delta T_O} + w_4 \frac{P_d}{P_{d,0}} + w_5 \sum_{k=1}^{8} \frac{P_k}{P_{K,0}} \qquad (63)$$

Φ	Multi-criteria objective function	dimensionless
F	Cumulative driver anger index	dimensionless
VDV	Whole-body vibration dose	$m/s^{1.75}$
Δ*T*	Ambulance delay	s
Pd	Patient discomfort index	%
Pk	Disease index for the k*k*-th group	variable
*w*1 to *w*5	Criterion weights	dimensionless

The calculation of the objective function for the seven scenarios is presented in Table 10. The results indicate that S5, with Φ = 1.33, exhibits the best performance, followed by S4 with Φ= 1.40.

Table 10: Calculation of the Multi-Criteria Objective Function for the Seven Scenarios

Scenario	$F/F0$	$VDV/VDV0$	$\Delta T/\Delta T0$	$Pd/Pd,0$	$\sum Pk/Pk,0$	Φ
S0	1.00	1.00	1.00	1.00	8.00	2.45
S1	0.58	0.77	0.58	0.58	5.12	1.58
S2	0.61	0.80	0.61	0.61	5.38	1.65
S3	0.67	0.79	0.66	0.67	5.81	1.75
S4	0.51	0.72	0.50	0.50	4.48	1.40
S5	0.48	0.70	0.47	0.47	4.25	1.33
S6	0.53	0.72	0.50	0.51	4.55	1.42

A sensitivity analysis of the objective function was performed by varying the weights within a range of ±50%, the results of which are presented in Table 11.

Table 11: Sensitivity Analysis of the Objective Function Weights

Weighting Scenario	S4	S5	Best
Original weights	1.40	1.33	S5
$w3$=0.40	1.38	1.30	S5
$w1$=0.40	1.42	1.36	S5
Equal weights	1.45	1.38	S5

The results indicate that S5, with Φ = 1.33, exhibits the best performance, followed by S4 with Φ = 1.40. The connection between optimization and the effects on patients and occupants is clearly evident in this function: S5, by reducing 41 speed bumps (from 80 to 39) and 57 speed humps (from 102 to 45), decreases the effective exposure from 100.4 to 48.0 a 52.2% reduction in biomechanical load. This reduction leads to a 51.7% decrease in driver anger, a 16.7% reduction in occupant VDV, a 53.1% reduction in ambulance delay, and a 45.5% improvement in CPR quality. The sensitivity analysis demonstrates that S5 is the best under all weighting schemes, whereas S4 exhibits the most stable performance. Therefore, if the objective is to maximize the reduction of patient harm, S5 is selected; if the objective is to achieve a balance between safety and operations, S4 is preferred.

4. Discussion

The findings of this study demonstrate that optimizing the number and location of speed bumps and speed humps can lead to a considerable reduction in the biomechanical load imposed on patients. Regarding patients with traumatic injuries, Lesenyeho et al. (2025), by examining the experiences of emergency medical personnel in South Africa, showed that 61.3% of respondents strongly believed that speed bumps can exacerbate the pain of patients with major fractures en route to the hospital. This finding is consistent

with the results of the present study, which associates a reduction in speed bumps with a 48.5% decrease in the composite spinal injury index.[11].

Regarding intubated patients and those with catheters, Lesenyeho et al. (2025) showed that 62.5% of emergency medical personnel believed that speed bumps can cause dislodgement of life-saving equipment such as intravenous lines and endotracheal tubes. This finding is fully aligned with the results of the present study, which demonstrates a 66.7% reduction in the probability of endotracheal tube displacement. Beom et al. (2018), in their simulation study, also confirmed that speed bumps lead to improper hand positioning and impair the effectiveness of CPR [11,21].

Regarding spinal patients, Munjin et al. (2011), in a retrospective case study in Chile, identified 46 patients with 52 spinal fractures, all of which occurred after traversing a speed bump in a vehicle. Of these patients, 95.7% were on a bus, and 95.5% were seated in the last row. Another study in Brazil (2024) reported 19 patients with thoracolumbar fractures caused by speed bumps, more than 50% of whom required surgery. These findings are consistent with the results of the present study, which associates a reduction in speed bumps with a 48.5% decrease in spinal injury [30,31].

Regarding cardiovascular patients, Cocco and Iselin (1992), in a clinical study of 22 patients with stable heart disease who were caught in a speed bump trap during ambulatory electrocardiogram recording, showed that all patients reported cardiac symptoms, increased heart rate, and frequent ventricular arrhythmias, and myocardial ischemia was observed in some patients. This finding is consistent with the results of the present study, which associates a reduction in speed bumps with a 42.6% decrease in cardiovascular risk. Shin et al. (2020) also showed that every 1-minute increase in emergency arrival time reduces the survival rate by 1.46% [32,33]

Regarding ambulance delay, Garcia et al. (2013), analyzing 600 routes in Spain, showed that the average delay per speed bump is between 1.4 and 4.3 seconds, and ambulances carrying patients deviate up to 1 kilometer to avoid speed bumps, resulting in delays of up to 40 seconds. Toronto Paramedic Services (2010) also stated that the delay caused by speed bumps is cumulative, with each obstacle increasing it, and can directly affect patient outcomes [34,35].

Regarding stroke patients, Hong and Kim (2024), citing ITE (2018) data, showed that a fire engine is delayed by 3 to 5 seconds and an ambulance carrying a patient by up to 10 seconds per speed bump. Karch et al. (1998) reported a 1% reduction rate per minute of delay [36,37,38].

Regarding occupants, Kyrollos et al. (2020), by installing sensors on the ambulance floor, showed a strong linear relationship ($r = 0.95$ to 0.96) between traversal speed and peak acceleration, with traversal at speeds above 20 km/h causing discomfort and above 30 km/h causing considerable discomfort. This finding is consistent with the results of the present study, which identifies the 7×50 cm speed bump as a cause of zero comfort for occupants [39].

5.Conclusion

This study was conducted to optimize the number and location of speed bumps and speed humps across 48 urban roadways in and to evaluate the effects of this optimization on patients, occupants, and drivers. For this purpose, a convolutional neural network was employed to determine the optimal number of obstacles, and the effects of their reduction on eight patient groups and on occupant and driver groups were then quantified using biomechanical and clinical models.

The results demonstrated that scenario S5, with 39 speed bumps and 45 speed humps, exhibits the best performance, followed by S4 with 41 speed bumps and 48 speed humps. Compared to the existing condition of 80 speed bumps and 102 speed humps, this scenario achieves a 51.3% reduction in the number of speed bumps and a 55.9% reduction in the number of speed humps. This reduction leads to a 51.7% decrease in the cumulative driver anger index, a 51.3% decrease in the number of locations where occupants experience zero comfort, and a 16.7% reduction in the whole-body vibration dose.

Among the eight patient groups, the greatest improvements were observed in intubated patients (a 66.7% reduction in the probability of endotracheal tube displacement), post-surgical patients (a 62.9% reduction in the probability of wound dehiscence), and pregnant women (a 75% reduction in placental shear stress). The smallest improvements were recorded in cardiovascular patients (a 42.6% reduction in the increase in systolic blood pressure) and stroke patients (an 11.8% improvement in survival probability). This difference indicates that the effectiveness of obstacle reduction depends on the pathological mechanism of each patient group, and that patients with acute mechanical injuries benefit the most.

The dynamic analysis using the reference vehicle demonstrated that although the road acceleration at speed bumps is 16.8 times that at speed humps, due to the effective damping of the suspension system, the actual acceleration on the vehicle seat is only 22.8 times greater, and the actual VDV is approximately 3.3 times greater. This means that the vehicle body acts as a strong mechanical filter and absorbs the majority of road vibration. However, for patients in an ambulance, who have weaker stabilization and a stiffer ambulance suspension, this damping will be less, and the effects of VDV can be considerably greater.

The optimization of speed bumps and speed humps can affect occupants and patients through three principal pathways. The first pathway is the reduction of vibration load: by reducing the number of speed bumps, the whole-body vibration dose (VDV), which is the ISO 2631-1 standard index for vibration exposure, decreases. This reduction is critical for patients with spinal injuries, intubated patients, and post-surgical patients, as vibration can lead to equipment dislodgement, pain exacerbation, and even wound dehiscence. The second pathway is the reduction of emergency delay: by reducing the number of speed bumps, the time for an ambulance to reach the hospital decreases. For stroke patients, every minute of delay is equivalent to 1.9 million neurons lost, and for cardiac patients, every minute of delay reduces the survival rate by 1%. The reduction in cumulative delay from 1,310 seconds to 615 seconds in scenario S5 improves the survival probability from 0.34 to 0.38. The third pathway is the reduction of mechanical shock: speed bumps, with high jerk (1,256 m/s^3), impose a sudden force on the body, whereas speed humps, with low jerk (12.46 m/s^3), apply the load gradually. Therefore, reducing speed bumps has a direct effect on safety, particularly for patients with acute injuries (fractures, spinal trauma, intubation).

The final policy recommendation is that in future traffic calming planning, reducing the number of speed bumps should take higher priority than reducing speed humps, as the contribution of speed bumps to generating driver anger and zero occupant comfort is far greater. Furthermore, optimizing the location and number of obstacles using artificial intelligence methods can lead to a balance between traffic safety and the comfort of patients and occupants.

Limitations and Future Work

This study is limited by the absence of field measurements of acceleration in real ambulances and by the use of literature-based reference values for biomechanical parameters. For future research, it is recommended that empirical accelerometer data and clinical patient outcomes be collected in collaboration with emergency services, and that the model be calibrated accordingly.

Informed Consent

Verbal informed consent was obtained from all experts who participated in this study.

Funding Declaration

This research received no specific grant from any funding agency in the public, commercial, or not-for-profit sectors.

Authors' Contribution Statement

All authors (Sayyedmehdi Hosseinikhah, Hamid Mirzahossein, Mohammad Ali Asadi, Ali Naderan) contributed equally to all stages of this research. These contributions include research design, data collection and analysis, development of neural network models, drafting of the original manuscript, critical review, and final editing of the scientific content. All authors have read and approved the final version of the manuscript.

Declaration of competing interest

The authors declare that they have no known competing financial interests or personal relationships that could have appeared to influence the work reported in this paper.

Data availability

Data will be made available on request

References

[1] Ewing, R. (2017). US traffic calming manual. Routledge.DOI: 10.4324/9781351179652.

[2] Litman, T. (1999). Traffic calming: benefits, costs and equity impacts (p. 7). Victoria, BC, Canada: Victoria Transport Policy Institute.

[3] ALemour, B., Badran, O., Alawein, A., Al-Mashaqbeh, O., Ahmad, S., & Al-Wahsh, Y. (2026). Impact of Non-Standard Road Bumps on Vehicle Suspension Dynamics, Ride Comfort, and Fatigue Life: A Comparative Study in Jordan. DOI:10.21203/rs.3.rs-10099508/v1.

[4] Pau, M., & Angius, S. (2001). Do speed bumps really decrease traffic speed? An Italian experience. Accident Analysis & Prevention, 33(5), 585-597.DOI: 10.1016/S0001-4575(00)00070-1.

[5] Antić, B., Pešić, D., Vujanić, M., & Lipovac, K. (2013). The influence of speed bumps heights to the decrease of the vehicle speed–Belgrade experience. Safety science, 57, 303-312. DOI:10.1016/j.ssci.2013.03.008.

[6] Kırbaş, U., & Karaşahin, M. (2018). Comparison of speed control bumps and humps according to whole-body vibration exposure. Journal of Transportation Engineering, Part A: Systems, 144(9), 04018054. DOI:10.1061/jtepbs.0000177.

[7] Federal Highway Administration [FHWA]. (2017). Traffic calming ePrimer: Module 3 and 5. U.S. Department of Transportation

[8] Ahn, K., & Rakha, H. (2009). A field evaluation case study of the environmental and energy impacts of traffic calming. Transportation Research Part D: Transport and Environment, 14(6), 411-424. DOI:

10.1016/j.trd.2009.01.007.

[9] Oluwatomini, O., Eustace, D., Brewick, P., & Walsh, K. Q. (2026). Modeling the impacts of physical vertical deflection traffic calming measures on speed, traffic volume, noise, emissions, and delay-A systematic review. Advances in Transportation Studies, 68, 341.

[10] Tainter, F., Fitzpatrick, C., Knodler Jr, M., Furth, P. G., & Dulaski, D. (2024). Speed Management and Emergency Response–a Synthesis Study.

[11] Lesenyeho, M. H., Nyam, Y. S., & van Straaten, M. M. (2025). The impact of speed humps on out-of-hospital transported patients: the experience of Emergency Medical Services personnel. International Journal of Emergency Services, 14(3), 294-306. DOI:10.1108/IJES-04-2024-0029.

[12] Öz, E., Küçükkelepçe, O., Kurt, O., Çavuş, A. C., & ÇAVUŞ, A. C. (2023). Effect of speed humps on ambulance delay. Cureus, 15(1). DOI:10.7759/cureus.33722.

[13] Pons, P. T., Haukoos, J. S., Bludworth, W., Cribley, T., Pons, K. A., & Markovchick, V. J. (2005). Paramedic response time: does it affect patient survival?. Academic Emergency Medicine, 12(7), 594-600. DOI: 10.1197/j.aem.2005.02.013.

[14] Blackwell, T. H., & Kaufman, J. S. (2002). Response time effectiveness: comparison of response time and survival in an urban emergency medical services system. Academic Emergency Medicine, 9(4), 288-295. DOI:10.1197/aemj.9.4.288.

[15] Wilde, E. T. (2013). Do emergency medical system response times matter for health outcomes?. Health economics, 22(7), 790-806. DOI: 10.1002/hec.2851.

[16] AN, N., & Si, S. (2007). Mechanical vibration and shock–evaluation of human exposure to whole body vibration–part 4: Guidelines for the evaluation of the effects of vibration and rotational motion on passenger and crew comfort in fixed-guideway transport systems. Mechanical Vibration and Shock–Evaluation of Human Exposure to Whole Body Vibration–Part 4: Guidelines for the Evaluation of the Effects of Vibration and Rotational Motion on Passenger and Crew Comfort in Fixed-Guideway Transport Systems.

[17] Griffin, M. J. (2012). Handbook of human vibration. Academic press.

[18] Mansfield, N. J. (2004). Human response to vibration. CRC press.

[19] Codur, M. Y., Kuskapan, E., Yurtbas, E., & Kayaci Codur, M. (2026). Experimental Analysis of the Adequacy of Speed Bumps in Terms of Driving Comfort. Future Transportation, 6(4), 156. DOI:10.3390/futuretransp6040156.

[20] Khorshid, E., Alkalby, F., & Kamal, H. (2007). Measurement of whole-body vibration exposure from speed control humps. Journal of sound and vibration, 304(3-5), 640-659.DOI: 10.1016/j.jsv.2007.03.013.

[21] Beom, J. H., Kim, M. J., You, J. S., Lee, H. S., Kim, J. H., Park, Y. S., ... & Chung, H. S. (2018). Evaluation of the quality of cardiopulmonary resuscitation according to vehicle driving pattern, using a virtual reality ambulance driving system: a prospective, cross-over, randomised study. BMJ open, 8(9), e023784. DOI: 10.1136/bmjopen-2018-023784.

[22] Roosa, J. R., Vadeboncoeur, T. F., Dommer, P. B., Panchal, A. R., Venuti, M., Smith, G., ... & Bobrow, B. J. (2013). CPR variability during ground ambulance transport of patients in cardiac arrest. Resuscitation, 84(5), 592-595. DOI: 10.1016/j.resuscitation.2012.07.042.

[23] Chung, T. N., Kim, S. W., Cho, Y. S., Chung, S. P., Park, I., & Kim, S. H. (2010). Effect of vehicle speed on the quality of closed-chest compression during ambulance transport. Resuscitation, 81(7), 841-847. DOI:10.1016/j.resuscitation.2010.02.024.

[24] Dewangan, D. K., & Sahu, S. P. (2020). Deep learning-based speed bump detection model for intelligent vehicle system using raspberry Pi. IEEE sensors journal, 21(3), 3570-3578. DOI:10.1109/JSEN.2020.3027097.

[25] Varma, V. S. K. P., Adarsh, S., Ramachandran, K. I., & Nair, B. B. (2018). Real time detection of speed hump/bump and distance estimation with deep learning using GPU and ZED stereo camera. Procedia computer science, 143, 988-997. DOI:10.1016/j.procs.2018.10.335.

[26] Menegazzo, J., & von Wangenheim, A. (2022). Speed bump detection through inertial sensors and deep learning in a multi-contextual analysis. SN Computer Science, 4(1), 18. DOI:10.1007/s42979-022-01438-w.

[27] Molan, A. M., & Kordani, A. A. (2014). Optimization of speed hump profiles based on vehicle dynamic performance modeling. Journal of transportation engineering, 140(8), 04014035. DOI:10.1061/(ASCE)TE.1943-5436.0000686.

[28] Celaya-Padilla, J. M., Galván-Tejada, C. E., López-Monteagudo, F. E., Alonso-González, O., Moreno-Báez, A., Martínez-Torteya, A., ... & Gamboa-Rosales, H. (2018). Speed bump detection using accelerometric features: A genetic algorithm approach. Sensors, 18(2), 443. DOI:10.3390/s18020443.

[29] Zhang, J., Wang, J., Zang, H., Ma, N., Skitmore, M., Qu, Z., ... & Chen, J. (2024). The application of machine learning and deep learning in intelligent transportation: A scientometric analysis and qualitative review of research trends. Sustainability, 16(14), 5879. DOI:10.3390/su16145879.

[30] Munjin, M. A., Zamorano, J. J., Marré, B., Ilabaca, F., Ballesteros, V., Martínez, C., ... & García, N. (2011). Speed hump spine fractures: injury mechanism and case series. Clinical Spine Surgery, 24(6), 386-389. DOI: 10.1097/BSD.0b013e3182019dda.

[31] Amorim, R. P., Henriques, V. M., Santos, L. L., Vasconcelos, F. A., Schmidt, A. M., Torrão, F. L., ... & Guedes, F. (2024). Thoracolumbar Fractures Due to Speed-Humps: A Case Series of Spine Fractures from an Atypical Cause of Injury. Arquivos Brasileiros de Neurocirurgia: Brazilian Neurosurgery, 43(04), e372-e377. DOI:10.1055/s-0045-1809636.

[32] Cocco, G., & Iselin, H. U. (1992). Cardiac risk of speed traps. Clinical cardiology, 15(6), 441-444. DOI: 10.1002/clc.4960150610.

[33] Shin, S. D., et al. (2020). The impact of emergency response time on survival rates of acute cardiac arrest patients. Korean Circulation Journal . DOI:10.22037/aaemj.v13i1.2596.

[34] Garcia, A., Moreno, A. N. A. T., Romero, M., & Perea, J. (2013). Estimating the effect of traffic calming measures on ambulances. Emergencias, 25(1), 285-288.

[35] Toronto Paramedic Services. (2010). Traffic calming measures - Wineva Avenue: Evaluation for the installation of speed humps and/or pinch points . City of Toronto

[36] Hong, K., & Kim, J. (2024). The Dilemma of Speed Bumps in Reducing Damage During Traffic Accidents. Journal of the Society of Disaster Information, 20(4), 828-839.DOI: 10.15683/kosdi.2024.12.31.828.

[37] Institute of Transportation Engineers. (2018). Guidelines for the design and application of speed humps. Institute of Transportation Engineers.

[38] Karch, S. B., Graff, J. P., & Young, S. (1998). Response times and outcomes for cardiac arrests in Las Vegas casinos. The American Journal of Emergency Medicine , 16 (3), 249-253. DOI: 10.1016/s0735-6757(98)90094-8.

[39] Kyrollos, D. G., Stachiw, T., Green, J. R., & Langlois, R. G. (2020). Injury risk and comfort assessment applied to ambulance transportation. In Proc. 7th Int. Conf. Cont. Syst. Robot (Vol. 10). DOI:10.11159/cdsr20.156.